SyNPL: Synthetic Notch pluripotent cell lines to monitor and manipulate cell interactions *in vitro* and *in vivo*.

Running title: Engineering cell interactions

Mattias Malaguti[1,‡], Rosa Portero Migueles[1], Jennifer Annoh[1], Daina Sadurska[1,2], Guillaume Blin[1], Sally Lowell[1,‡]

1. Centre for Regenerative Medicine, Institute for Stem Cell Research, School of Biological Sciences, University of Edinburgh, 5 Little France Drive, Edinburgh EH16 4UU, UK
2. Current address: Sir William Dunn School of Pathology, University of Oxford, Oxford, United Kingdom

‡ Authors for correspondence: mattias.malaguti@ed.ac.uk sally.lowell@ed.ac.uk

Keywords: Cell interaction; SynNotch; pluripotent stem cells; cell engineering, patterning.

SUMMARY STATEMENT

Optimised Synthetic Notch circuitry in mouse pluripotent stem cells provides a modular tool to monitor cell-cell interactions and program synthetic patterning of cell fates in culture and in embryos.

ABSTRACT

Cell-cell interactions govern differentiation and cell competition in pluripotent cells during early development, but the investigation of such processes is hindered by a lack of efficient analysis tools. Here we introduce SyNPL: clonal pluripotent stem cell lines which employ optimised Synthetic Notch (SynNotch) technology to report cell-cell interactions between engineered "sender" and "receiver" cells in cultured pluripotent cells and chimaeric mouse embryos. A modular design makes it straightforward to adapt the system for programming differentiation decisions non-cell-autonomously in receiver cells in response to direct contact with sender cells. We demonstrate the utility of this system by enforcing neuronal differentiation at the boundary between two cell populations. In summary, we provide a new tool which could be used to identify cell interactions and to profile changes in gene or protein expression that result from direct cell-cell contact with defined cell populations in culture and in early embryos, and which can be adapted to generate synthetic patterning of cell fate decisions.

INTRODUCTION

During embryogenesis, pluripotent cells undergo a series of cell fate decisions that are controlled by interactions between epiblast cells, their early differentiated derivatives, and the surrounding extraembryonic tissues (Arnold and Robertson, 2009; Nowotschin and Hadjantonakis, 2010; Rossant and Tam, 2009). The transcriptional changes that accompany exit from pluripotency and differentiation into specific cell types have been extensively characterised, and the long-range signals that control these changes are now well understood (De Los Angeles et al., 2015; Kinoshita and Smith, 2018; Pera and Tam, 2010; Posfai et al., 2021; Tam and Loebel, 2007). Less is known about how early developmental decisions are influenced by direct interactions of cells with their neighbours. Cell-cell interactions play a key role in development (Dias et al., 2014; Gurdon, 1987; Johnson and Ziomek, 1983; Schultz, 1985), but until recently there has been a paucity of molecular and technological tools available to study these processes in detail in relevant settings (Nishida-Aoki and Gujral, 2019; Yang et al., 2021).

Quantitative image analysis can be used to identify and infer the effect of neighbours on the properties of cells of interest in fixed samples (Blin et al., 2018; Fischer et al., 2020; Forsyth et al., 2021; Toth et al., 2018). We have recently developed a software suite for automated neighbour identification during live imaging (Blin et al., 2019), which provides researchers with a further dimension to study the effects on cell-cell interactions on cell fate decisions. Whilst live image analysis provides high-resolution visual information, this approach is labour-intensive and only leads to neighbour identification *a posteriori*.

The field of Synthetic Developmental Biology (Davies, 2017; Ebrahimkhani and Ebisuya, 2019; Ho and Morsut, 2021; Santorelli et al., 2019; Schlissel and Li, 2020) seeks to understand the mechanisms of patterning and cell differentiation through the engineering of genetic circuits (Cachat et al., 2016; Matsuda et al., 2015; Sekine et al., 2018). By re-engineering the Notch/Delta signalling cascade (Figure 1A), Lim and colleagues generated a synthetic circuit capable of reporting and manipulating cell-cell interactions in real time (Morsut et al., 2016). A "sender" cell presenting an extracellular membrane-bound antigen of interest is recognised by a "receiver" cell expressing a chimaeric Synthetic Notch (SynNotch) receptor, composed of an extracellular antigen-recognition domain, the Notch1 core transmembrane domain containing proteolytic cleavage sites, and an intracellular synthetic effector

domain (Fig. 1B-D). The modularity of SynNotch circuitry makes it possible to interrogate and manipulate the effects of interactions between cell types of interest.

SynNotch technology has been used for monitoring cell-cell interactions, generating synthetic patterns, generating synthetic morphogen gradients, inducing contact-mediated gene editing, and generating custom antigen receptor T-cells (Cho et al., 2018; Choe et al., 2021; He et al., 2017; Huang et al., 2020; Roybal et al., 2016; Sgodda et al., 2020; Toda et al., 2018; Toda et al., 2020; Wang et al., 2021). SynNotch technology has been established in *Drosophila* (He et al., 2017) as well as in immortalised cell lines and differentiated cell types, but its potential in the study of mammalian developmental events remains largely untapped.

Mouse embryonic stem cells (ESCs) can be differentiated into any cell type *in vitro*, can give rise to chimaeric embryos and can be used to establish transgenic mouse lines (Bradley et al., 1984; Evans and Kaufman, 1981; Martin, 1981). Adapting the SynNotch system for use in mouse ESCs would therefore permit monitoring and manipulation of cell-cell interactions in a developmental context both *in vivo* and *in vitro*. The original system designed by (Morsut et al., 2016) used lentiviral transduction of immortalised and primary cell lines, where transgene expression was driven from the retroviral SFFV promoter. Lentiviral transduction can lead to multiple copy transgene integration in mouse ESCs (Pfeifer et al., 2002), and the SFFV promoter is prone to silencing in mouse pluripotent cells and their derivatives (Herbst et al., 2012; Pfaff et al., 2013; Wu et al., 2011), making this system suboptimal for mouse ESCs.

In this study, we made several adaptations to the original SynNotch system (Morsut et al., 2016) to establish clonal modular SynNotch pluripotent cell lines (SyNPL). We characterised the SyNPL system by monitoring interactions between EGFP-expressing sender cells and mCherry-inducible receiver cells *in vitro*, then showed that this system can report interactions between neighbouring cells *in vivo* in chimaeric mouse embryos, that it can be used for synthetic patterning, and that its modular design can be exploited to conveniently manipulate cell-cell interactions and drive contact-mediated synthetic cell fate engineering.

RESULTS

Design of SyNPL ESCs

We adapted the SynNotch system, which was previously established through viral transduction of immortalised mouse L929 fibroblasts and K562 erythroleukaemic cells (Morsut et al., 2016), for use in mouse ESCs. In this system, sender cells are labelled with membrane-tethered extracellular EGFP (Fig. 1B). Receiver cells constitutively express a SynNotch receptor composed of an anti-GFP nanobody (LaG17) (Fridy et al., 2014), the mouse Notch1 minimal transmembrane core (Uniprot: Q01705, residues 1427-1752), and a tetracycline transactivator (tTA) (Gossen and Bujard, 1992), and contain a tetracycline response element (TRE) promoter capable of driving *mCherry* expression in response to tTA binding (Fig. 1C). Interaction of EGFP on sender cells with the anti-GFP nanobody on receiver cells leads to cleavage of the Notch1 core, releasing the tTA which can translocate to the nucleus, bind to the TRE promoter and drive *mCherry* expression (Fig. 1D). In addition, we constitutively labelled receiver cells with a tagBFP-3xNLS construct (Fig. 1C,D) to conveniently identify them by fluorescence microscopy and flow cytometry even in the absence of a contact-dependent mCherry signal.

Our aims when adapting the SynNotch system were to generate ESC lines with low cell-cell variability, robust and sustained transgene expression, and a modular design to allow convenient transgene

106 exchange. In order to avoid cell-cell variability we generated clonal cell ESC lines with stable genomic
107 integration of the SynNotch system components, delivering transgenes by electroporation rather than
108 lentiviral transduction (Boggs et al., 1986; Charrier et al., 2011; Pfeifer et al., 2002; Smithies et al.,
109 1985). We sought to ensure uniform levels of transgene expression by screening clonal lines and/or
110 targeting transgenes to specific genomic locations, and by replacing the silencing-prone SFFV
111 retroviral promoter used by (Morsut et al., 2016) with CAG (Niwa et al., 1991) or mouse *Pgk1*
112 (McBurney et al., 1991) promoters, which have been extensively characterised in mouse ESCs (Chen
113 et al., 2011; Hong et al., 2007). Finally, we introduced modularity to our system by generating a
114 "landing platform" master cell line to allow recombination-mediated cassette exchange (RMCE) of
115 transgenes of interest.

116 **Generation of extracellular membrane-tethered EGFP-expressing sender ESCs**

117 We first generated clonal sender cell lines expressing membrane-tethered extracellular EGFP. The CAG
118 and mouse *Pgk1* promoters are both silencing-resistant promoters commonly used to drive ubiquitous
119 transgene expression in ESCs (Herbst et al., 2012; Liew et al., 2007). We asked which of these
120 promoters can generate sender cells with strong and uniform expression of membrane EGFP. We also
121 explored whether EGFP molecules with HA and Myc protein tags can retain "sender" function in
122 pluripotent cells.

123 We electroporated mouse ESCs with four alternative sender constructs, containing either CAG or
124 mouse *Pgk1* promoters driving expression of either untagged or HA- and Myc-tagged EGFP fused to a
125 membrane-tethering domain (Fig. 2A-D). We isolated and expanded 64 clonal lines derived from
126 stable genomic integration of the four constructs, and screened them by flow cytometry, analysing
127 median EGFP intensity (Fig. 2E,F), percentage of EGFP-positive cells (Fig. 2G,H) and EGFP distribution
128 (Figs. S1, S2). Both CAG and *Pgk1* promoters drive high uniform expression of EGFP, and, as expected,
129 there is considerable variability in EGFP expression between clonal lines.

130 We selected one untagged EGFP sender clone (CmGP1) and one HA- and Myc-tagged EGFP sender
131 clone (CHmGMP19), exhibiting high, uniform and similar levels EGFP expression (Fig. 2I) for further
132 analysis. For both clones, the pattern of EGFP expression was consistent with membrane localisation,
133 and, in the case of the HA- and Myc-tagged CHmGMP19 clone, the pattern of HA and Myc expression
134 coincided with that of EGFP (Fig. 2J).

135 **Generation of a safe harbour site landing pad master ESC line**

136 To facilitate convenient and repeated modification of the genome, we generated a clonal ESC line
137 carrying a "landing pad" targeted to the *Rosa26* locus, a safe harbour site in the mouse genome
138 (Friedrich and Soriano, 1991). This landing pad contains a splice acceptor, the *Neo* (G418/geneticin
139 resistance) gene, and a CAG promoter driving expression of *mKate2-3xNLS*, which encodes a red
140 fluorescent protein with no evident phenotypic effect in mouse embryos (Malaguti et al., 2013;
141 Shcherbo et al., 2009). This entire cassette is flanked by two *attP50* sites, which allows for ϕC31
142 integrase-mediated recombination with cassettes flanked by two *attB53* sites (Huang et al., 2009;
143 Tosti et al., 2018) (Fig. S3A). After confirming insertion at the correct genomic locus (Fig. S3B), we
144 verified that all cells express high and uniform levels of mKate2-3xNLS (Fig. S3C,D). We named this cell
145 line EM35.

146 **An "all-in-one" design fails to generate fully functional mCherry inducible receiver cells**

147 We first asked whether it is possible to target all transcriptional units required for receiver cell activity
148 to the *Rosa26* landing pad in EM35 ESCs, and whether this would lead to the generation of functional

149 receiver ESCs. Design and characterisation of the resulting cell lines is explained in detail in
150 Supplementary Methods and Figs. S4-S9. Briefly, mCherry could, as expected, be induced by
151 subpopulations of tagBFP-positive receiver cells in response to interaction with EGFP-positive sender
152 cells, but this receiver cell design was hampered by variable levels of tagBFP, variable inducibility of
153 mCherry, and low levels of the SynNotch receptor. We conclude that the SynNotch receptor construct
154 and *TRE-mCherry* cassette can function as expected in ESCs, but further modifications to the design
155 are required to obtain a reliable contact-reporting system.

156 **A multi-step design produces fully functional mCherry-inducible receiver ESCs**

157 We hypothesised that two independent events may be affecting mCherry inducibility in "all-in-one-
158 locus" receiver cells (Figs. S4-S9). Firstly, *mCherry* and *tagBFP* transgenes may have been lost due to
159 mitotic recombination (Stern, 1936) or errors in replication at similar DNA sequences in close
160 proximity (*Pgk1* promoters, *bGHpA* signals). Secondly, the SynNotch receptor may not be expressed
161 at high enough levels (Fig. S9).

162 We circumvented potential loss of DNA by physically separating the three transcriptional units through
163 random genomic integration of the SynNotch receptor and *tagBFP-3xNLS* cassettes, and by removing
164 identical DNA sequences. To increase levels of SynNotch receptor and obtain uniform levels of tagBFP-
165 3xNLS, we added an internal ribosome entry site (IRES) followed by *Ble* (zeocin resistance gene)
166 downstream of the SynNotch receptor sequence, and an IRES followed by *Hph* (hygromycin B
167 resistance gene) downstream of the *tagBFP-3xNLS* sequence (Fig. 3A).

168 We first randomly integrated the SynNotch receptor construct into the genome of EM35 landing pad
169 ESCs (Fig. S10A). We selected two clones (35SRZ9, 35SRZ86) with high, uniform Myc expression (Fig.
170 S10B). The levels of Myc in these clones were higher than those in receiver cells generated with an all-
171 in-one design (clones SNCB+4 and SNCB-6) and higher than those in Myc-tagged sender cells
172 (CHmGMP19) (Fig. S10C). We then randomly integrated the *tagBFP-3xNLS* transgene into the genome
173 of these two clones (Fig. S10D). We selected one clone for each parental line with high, uniform
174 expression of tagBFP-3xNLS (PSNB-A clone 10, PSNB-B clone 3) (Fig. S10E,F). We renamed these lines
175 PSNB (Parental SynNotch tagBFP) clones A and B respectively.

176 Next, we performed RMCE at the *Rosa26* landing pad in PSNB cells to replace the *mKate2* transgene
177 with one of three constructs: the *TRE-mCherry* cassette present in the SCNB construct, a *tetO-mCherry*
178 cassette with more tTA binding sequences elements in the inducible promoter (to test whether this
179 led to improved mCherry induction), or an empty vector cassette to generate tagBFP-positive mKate2-
180 and mCherry-negative control cell lines (Fig. S11A). We verified that integration of the empty vector
181 cassette led to loss of mKate2 expression, and used these control cell lines to confirm that tagBFP
182 signal was able to unambiguously identify receiver cells (Figs. 3B,C, S11B).

183 We then asked whether the new receiver cell lines containing inducible mCherry cassettes expressed
184 mCherry in response to co-culture with sender cells. We screened 27 clones for tagBFP and mCherry
185 expression by culturing them in the presence or absence of sender cells for 24 hours (Fig. S11C-G). We
186 observed that all genetically identical clones behaved very similarly, suggesting we were not
187 experiencing silencing or loss of DNA. Clones containing the larger *tetO-mCherry* cassette exhibited
188 high levels of mCherry leakiness in the absence of sender cells. Co-culture with sender cells led to
189 mCherry induction, but the distributions in the presence and absence of sender cells overlapped
190 significantly (Fig. S11D,F,G). Clones containing the smaller *TRE-mCherry* cassette exhibited mCherry
191 leakiness in the absence of sender cells, however co-culture with sender cells led to an increase in
192 mCherry expression to levels which displayed minimal overlap with those seen in cells cultured in the

193 absence of sender cells (Fig. S11C,E,G). Leakiness in the absence of sender cells can be reduced, but
194 not abolished, by treatment of cells with the γ-secretase inhibitor DAPT (which inhibits cleavage of the
195 SynNotch receptor) or with doxycycline (which inhibits tTA-driven transcription) (Fig. S12A,B).

196 We selected three clones with minimal leakiness and high inducibility for downstream analysis
197 (PSNBA-TRE1, PSNBB-TRE10, PSNBB-TRE9). We renamed these cells STC (for SynNotch-TRE-mCherry)
198 clones A1, B1 and B2 respectively. These receiver lines induced mCherry after co-culturing sender and
199 receiver cells together for 24 hours. mCherry was specifically induced in tagBFP-positive receiver cells
200 that were in contact with EGFP-positive sender cells (Fig. 3D). We confirmed that mCherry is robustly
201 induced in the majority of tagBFP-positive receiver cells following co-culture with 9-fold excess of
202 CmGP1 sender cells at confluence (Fig 3B,C,E,F).

203 These observations demonstrate that physical separation of the three transcriptional units in the
204 genome of receiver cells, coupled to the use of internal ribosome entry sites and selectable markers
205 within the units, can lead to the generation of receiver ESC lines which exhibit clear and specific
206 induction of mCherry upon interaction with EGFP-expressing sender cells.

207 **Extracellular membrane-tethered EGFP is required for contact-mediated transgene induction in**
208 **receiver cells**

209 It would be useful to make use of existing GFP fluorescent reporter ESCs (for example, cell-state
210 reporters or signalling reporters) to act as sender cells, in order to test how particular cell states may
211 influence direct neighbours. However, many such cell lines make use of non-membrane-tethered GFP,
212 which seems unlikely to interact with the anti-GFP nanobody on STC receiver cells. We therefore
213 wished to test whether membrane tethering of EGFP to the extracellular space was absolutely
214 necessary for effective neighbour-labelling.

215 We cultured STC receiver cells alone (Fig. 3E), in the presence of CmGP1 sender cells (Fig. 3F), in the
216 presence of a control cell line expressing untagged intracellular EGFP (E14GIP1) (Fig. 3G), or in the
217 presence of CmGP1 sender cells containing an extra untagged intracellular EGFP transgene
218 (CmGP1GH1) (Fig. 3H). E14GIP1 cells, which do not express membrane-tethered EGFP, did not induce
219 mCherry above baseline levels in in co-cultured STC receiver cells (Fig. 3E-G). mCherry is induced to
220 similar levels following co-culture with either CmGP1 or CmGP1GH1 sender cells (Fig. 3F,H), suggesting
221 that the additional untagged EGFP transgene in CmGP1GH1 cells does not interfere with mCherry
222 induction. We conclude that cells containing intracellular GFP cannot function as sender cells unless
223 supplemented with extracellular membrane-tethered EGFP.

224

225 **tagBFP-3xNLS lineage label allows identification of EGFP cross-labelled receiver cells**

226 In other cell types, a membrane-tethered anti-GFP nanobody can bind and internalise membrane-
227 tethered GFP on neighbouring cells (Tang et al., 2020). This is also the case in ES cells (Fig. S12B):
228 punctuate EGFP signal is visible in mCherry-expressing activated receiver cells (Fig. S12C). It could
229 therefore be difficult to unambiguously separate of STC receiver cells from CmGP1 sender cells by flow
230 cytometry based on EGFP expression alone (Fig. S12D). This problem is overcome by using the tagBFP-
231 3xNLS lineage label in STC receiver cells (Fig. S12E). Furthermore, separation of sender and receiver
232 cells based on EGFP alone can be achieved by using CmGP1GH1 sender cells, which contain a second
233 EGFP transgene, leading to increased separation between sender cells and cross-labelled receiver cells
234 (Fig. S12F,G).

235 **Increasing sender:receiver cell ratios leads to increased transgene induction in receiver cells**

236 We next asked how differing sender:receiver cell ratios affect the efficiency of neighbour-labelling.
237 We co-cultured STC receiver cells with different proportions of sender cells for 24 hours (Fig. S13). We
238 observed that as few as 20% of sender cells were sufficient to induce mCherry in approximately half
239 of STC receiver cells, and that 90% sender cells could induce mCherry in over 90% of STC receiver cells
240 (Fig. S13A,B). mCherry fluorescence follows a bimodal distribution in receiver cells exposed to "non-
241 saturating" numbers of sender cells, and a unimodal distribution in receiver cells exposed to
242 "saturating" numbers of sender cells (Fig. S13C-H). This suggests that STC receiver cells which have
243 come into contact with sender cells can uniformly induce high levels of mCherry expression when co-
244 culturing cells at a 9:1 sender:receiver cell ratio (Fig. S13I-K).

245

246 **Kinetics of contact-dependent transgene induction in receiver cells**

247 We next performed time-lapse microscopy. In order to capture a range of behaviours, we co-cultured
248 CmGP1GH1 sender cells with STC receiver cells at a 1:1 sender:receiver ratio at moderate density, and
249 filmed cells for 24 hours (Fig. 4A, Movie 1). mCherry first became visible 5-6 hours after initial sender-
250 receiver contact (Fig. 4A, yellow arrowheads). We observed STC receiver cells which did not make
251 contact with sender cells and remained mCherry-negative (Fig. 4A, magenta arrowheads), and an STC
252 receiver cell that made contact with a sender cell 2 hours before the cells were fixed at the 24-hour
253 timepoint for immunofluorescence, and which remained mCherry-negative (Fig. 4A, cyan
254 arrowheads).

255 We then quantified the kinetics of mCherry induction. We co-cultured 10% STC receiver cells with 90%
256 sender cells at high density in order to ensure interaction of almost every receiver cell with at least
257 one sender cell (Fig. 4B, Movie 2), and analysed mCherry expression in receiver cells by flow cytometry
258 over the course of 72 hours (Figs. 4C-E, S14A,B), and by live imaging and tracking of individual cells
259 over the course of 24 hours (Figs. 4B,F,G, S14C-H). mCherry is first induced at low levels at around 5
260 hours (Figs. 4D-G, S14 A-H) and increases until around 48 hours (Figs 4 D-H, S14 A-B).

261

262 **Minimum time of contact required for transgene induction**

263 Relying on direct detection of mCherry (Fig 4C-G) is likely to overestimate the minimum duration of
264 cell contact required for mCherry induction because mCherry protein maturation will introduce a
265 time-lag between initiation of mCherry transcription and the detection of mCherry fluorescence.
266 Indeed, time-lapse analysis (Fig. 5A, Movie 3) provides an example of an STC receiver cell which
267 remained in contact with a sender cell for 8 hours, lost contact for 12 hours following a cell division,
268 but continued to increase mCherry expression after losing contact (Fig. 5A, white arrowheads).

269 We designed an experimental strategy to overcome this problem. We co-cultured 10% STC receiver
270 cells with 90% CmGP1 sender cells for various time points between 0 and 24 hours, then added
271 doxycycline to the culture medium for a further 16 hours (Fig. 5B). Doxycycline prevents tTA from
272 binding to *TRE* sequences (Gossen and Bujard, 1992), hence we expect doxycycline administration to
273 halt *mCherry* transcription in receiver cells while still allowing time for mCherry protein to mature.
274 This means that any mCherry signal observed after doxycycline administration should be ascribable to
275 cell-contact-dependent transcription that took place during the initial period of co-culture in
276 doxycycline-free medium. In this experimental setting, we observed low but detectable induction of
277 mCherry when cells had experienced only 2 hours of doxycycline-free co-culture (Figs. 5C,D, S15).

These data collectively suggest that 2 hours of sender-receiver contact may be sufficient for induction of low levels of mCherry, and that mCherry levels will keep increasing in receiver cells for a period of time following the loss of sender-receiver contact. This neighbour-labelling system can therefore identify receiver cells that have had relatively brief interactions with sender cells or which have recently lost contact with sender cells.

Kinetics of contact-dependent mCherry perdurance in receiver cells

We next established how long mCherry signal persists following loss of tTA-mediated *mCherry* transcription. We co-cultured 10% STC receiver cells with 90% CmGP1GH1 cells for 24 hours, then added doxycycline to the culture medium (to block the activity of tTA and halt *mCherry* transcription) and filmed the cells over 48 hours (Fig. S16A,B, Movies 4,5). mCherry fluorescence barely changed for the initial 8-12 hours, then gradually decreased until extinguishment around 38-40 hours after doxycycline addition (Fig. S16A,B). To quantify this process, we co-cultured 10% STC receiver cells with 90% CmGP1 sender cells for 24 hours, then added doxycycline to the culture medium and analysed mCherry fluorescence by flow cytometry at various timepoints (Fig. S16C). No reduction of mCherry signal was observed for the initial 8 hours following doxycycline administration, then median mCherry expression decreased by approximately half at 16 hours, and returned to background levels within 48 hours (Fig. S16D-F). Quantification of live imaging data at hourly timepoints broadly confirmed these observations, with mCherry levels halving after approximately 20-24 hours, and mCherry signal returning to background levels around 48 hours (Fig. S16G).

Taken together, these results suggest that induction of mCherry occurs more rapidly than loss of mCherry signal, presumably due to the high stability of this fluorescent protein, confirming the utility of this system for identifying recent as well as current cell-cell interactions.

The SyNPL SynNotch cell-cell interaction reporter is functional in early mouse embryos

We asked if the SyNPL system could function *in vivo* in early mouse embryos. We aggregated wild-type morulae with CmGP1GH1 sender cells and/or STC receiver cells, and cultured these to the blastocyst stage (Fig. 6). As expected, all chimaeric blastocysts (80/80) containing both sender and STC receiver cells induced expression of mCherry, whereas no wild-type blastocysts nor blastocysts containing only sender cells displayed mCherry expression (Fig. 6A,B). 18 out of 19 chimaeras containing STC receiver cells alone did not express readily detectable levels of mCherry (Fig. 6B), in line with the low proportion of mCherry-high cells observed *in vitro* in STC receiver cells cultured alone. Treatment of chimaeric embryos with the γ-secretase inhibitor DAPT suppressed mCherry induction, and withdrawal of DAPT allowed mCherry upregulation (Fig. S17), confirming that SynNotch receptor cleavage is required for mCherry induction.

All three STC clonal lines reliably induced mCherry within chimaeric embryos that also contained CmGP1GH1 sender cells (Fig. 5B, Fig. S18A), with mCherry generally appearing within 20h of aggregation (Movie 6). As expected, some receiver cells remain unlabelled when given limited access to sender cells within chimeric blastocysts (aggregations performed with eight receiver cells and only one sender cell: Fig. S18B), in keeping with the contact-dependent nature of SynNotch activation. Post-implantation chimaeras containing both sender and receiver cells displayed mCherry induction throughout the body axis (Fig. S18C). These results suggest that the SyNPL neighbour-labelling system is functional, efficient and reliable *in vivo*.

Spatial confinement of sender and receiver cells leads to synthetic patterning

320 SynNotch technology has been successfully employed to generate synthetic patterns. Strategies to
321 achieve this include co-culturing cells in a low sender:receiver cell ratio in order to create 2-
322 dimensional activated receiver cell rings surrounding a clone of sender cells (Morsut et al., 2016),
323 creating self-organising cell aggregates through contact-mediated induction of adhesion molecules
324 (Toda et al., 2018), and recreating morphogen gradients through the use of anchor proteins to capture
325 diffusible receiver cell-activating signal (Toda et al., 2020).

326 We asked if we could generate a synthetic stripe of transgene expression at the region of contact
327 between sender and receiver cells. We plated CmGP1 sender and STC receiver cells in separate
328 chambers of a removable multi-chamber cell culture insert and allowed them to reach confluence. We
329 then removed the insert, allowing cells to grow in the space between chambers and make contact
330 (Fig. 7A; a detailed description of stripe generation and characterisation can be found in
331 Supplementary Methods and in Fig. S19). A distinct stripe of mCherry expression appeared at the
332 sender:receiver border (Fig. 7B) 24 hours after initial sender:receiver contact. This demonstrates that
333 SynNotch technology can be successfully employed in mouse ESCs to generate synthetic patterns of
334 gene expression.

335 **Harnessing modularity of SyNPL SynNotch ESCs to synthetically alter cell fate**

336 The modularity of our SyNPL SynNotch system design makes it straightforward to generate clonal
337 receiver cell lines with inducible expression of any gene of interest.

338 The transcription factor Neurog1 (Neurogenin 1) drives neuronal differentiation of progenitor cells
339 during mouse development (Cau et al., 2002; Ma et al., 1998; Yuan and Hassan, 2014). Ectopic
340 expression of Neurog1 is sufficient to drive neuronal differentiation (Cai et al., 2000; Ma et al., 1996)
341 even in mesodermal tissues (Perez et al., 1999) and in mouse ESCs cultured in pluripotent culture
342 conditions (Velkey and O'Shea, 2013). We asked whether a TRE-inducible Neurog1 transgene in
343 receiver cells would drive neuronal differentiation as a specific response to contact with sender cells.

344 We generated STN (SynNotch TRE-Neurog1) receiver cells by performing RMCE at the *Rosa26* landing
345 pad in PSNB cell lines to replace the *mKate2-3xNLS* transgene with a *TRE-3xFlag-Neurog1* cassette
346 (Figs. 7C, S20A). We co-cultured STN receiver cells with CmGP1 senders cells for 48 hours, the
347 timepoint at which we observed maximum mCherry induction in STC receiver cells (Figs. 4C,D, S14A,B).
348 We confirmed this resulted in robust induction of 3xFlag-Neurog1 in STN receiver cells compared to
349 STN receiver cells cultured alone (Fig. S20B).

350 We then asked whether we could induce contact-mediated neuronal differentiation of receiver cells
351 in pluripotent culture conditions, and whether we could engineer differentiation to occur in a
352 synthetic pattern. We repeated the synthetic stripe patterning experiment described above (Fig.
353 7A,B), using STN receiver cells in place of STC receiver cells. We assessed the expression of the
354 neuronal marker Tubb3 96 hours after initial sender:receiver contact, and observed evident induction
355 of Tubb3 and acquisition of neuronal morphology by STN receiver cells at the sender:receiver border
356 (Fig. 7D). We verified that E14GIP1 cytoplasmic EGFP control cells were unable to induce neuronal
357 differentiation at the border with STN receiver cells (Fig. S21A). We observed that Neurog1 is induced
358 shortly after initial sender:receiver cell contact (Fig. S21B), and that Tubb3 induction first occurs 48
359 hours after initial interaction between sender and STN receiver cells (Fig. S21C).

360 We conclude that the interaction between EGFP-expressing sender cells and STN receiver cells can
361 lead to contact-mediated *Neurog1* induction and neuronal differentiation of receiver cells in non-
362 permissive culture conditions. This demonstrates that the SyNPL system can be readily used to
363 generate clonal ESC lines for contact-mediated induction of transgenes of interest, and that these cell

364 lines can in turn be used to manipulate cell-cell interactions in order to program synthetic cell fate
365 decisions in response to contact with a particular cell population at desired locations in space.

366

367 **DISCUSSION**

368 Engineering SynNotch machinery (Morsut et al., 2016) into pluripotent cells opens up many
369 opportunities for understanding how direct cell-cell interactions between neighbouring cells can
370 control differentiation decisions, mediate cell competition (Sancho et al., 2013) and orchestrate
371 morphogenesis (Gorfinkiel and Martinez Arias, 2021) as cells differentiate in 2D or 3D culture. Mouse
372 ES cells can contribute to chimaeric embryos, meaning that appropriately engineered cell lines can
373 also be used to understand and control cell-cell interactions during early embryonic development.
374 There are however particular challenges associated with engineering existing SynNotch technologies
375 into pluripotent cells. Here we describe how we overcame these challenges to generate the SyNPL
376 system: a set of clonal SynNotch "sender" and "receiver" mouse ES cells engineered with optimised
377 and modular SynNotch technology. We demonstrate the utility of the SyNPL system for monitoring
378 cell-cell interactions both in culture and in early mouse embryos, and show that we can use this system
379 to engineer contact-dependent cell fate decisions at the boundary between two populations of
380 pluripotent cells.

381 **Properties of sender cells**

382 We generated sender cell lines expressing high and uniform levels of extracellular membrane-
383 tethered EGFP. This transgenic construct was previously used for SynNotch sender cells (Morsut et
384 al., 2016; Sgodda et al., 2020), and comprises EGFP fused to an N-terminal mouse IgGK signal
385 sequence and a C-terminal human PDGFRB transmembrane domain. The addition of HA and Myc
386 tags at the N- and C-termini of EGFP did not affect the ability of sender cells to induce mCherry
387 expression in STC receiver cells (Fig. S13), so these epitope tags could be helpful for unequivocally
388 identifying and isolating sender cells.

389 Furthermore, the LaG17 anti-GFP nanobody can also bind to *Aequorea victoria* YFP, CFP and BFP, and
390 *Aequorea macrodactyla* CFP (Fridy et al., 2014), so membrane-tethered versions of these fluorophores
391 could likely be used to induce transgene induction in our receiver cells.

392 It would be interesting to test whether other cell lines labelled with lipid anchor-tethered GFP (Kondoh
393 et al., 1999; Nowotschin et al., 2009; Rhee et al., 2006; Shioi et al., 2011) could function as SynNotch
394 sender cells; this would require extracellular GFP localisation and generation of sufficient tensile force
395 upon receptor interaction (Morsut et al., 2016). GPI anchors GFP to the outer leaflet of the plasma
396 membrane (Rhee et al., 2006; Sevcsik et al., 2015); GFP-GPI-labelled cells should therefore be capable
397 of acting as sender cells. This does indeed appear to be the case in *Drosophila* (He et al., 2017).

398 **"All-in-one" locus receiver cells display suboptimal functionality**

399 Attempts at generating "all-in-one" *Rosa26*-targeted receiver cells (termed SNCB+ and SNCB- cells)
400 were unsuccessful. The large variation in tagBFP expression and low proportion of mCherry-inducible
401 ESCs in all clonal lines suggests that either widespread transgene silencing or loss of DNA occurred at
402 the *Rosa26* safe harbour locus in pluripotent cells. Furthermore, rederivation of clonal lines following
403 fluorescence-activated cell sorting of single SNCB+ and SNCB- cells led to re-establishment of the initial
404 heterogeneous distributions of fluorophore expression (Figs. S7, S8), suggesting that the all-in-one
405 design is not optimal for use in pluripotent cells. We were able to overcome these problems by
406 switching to a random-integration strategy, but it is possible that inclusion of IRES-antibiotic resistance

407 cassettes and/or insulator sequences may provide an alternative route towards generating a reliable
408 system without sacrificing the all-in-one-locus approach.

409 **Landing pad ESCs provide system modularity**

410 Targeting of a landing pad to the *Rosa26* safe harbour locus is an efficient strategy for rapid generation
411 of multiple cell lines through RMCE (Seibler et al., 2005; Tchorz et al., 2012; Tosti et al., 2018). Our cell
412 lines, harbouring a *Rosa26-attP50-Neo-mKate2-attP50* landing pad, make it straightforward to target
413 different transgenes to the same genomic locus in the same parental cell line. Our parental PSNB lines
414 harbouring the *Rosa26* landing pad allowed us to initially test the functionality of SynNotch in ESCs
415 with an inducible *mCherry* transgene in STC receiver cells, prior to generating genetically equivalent
416 STN receiver cells with a *Neurog1* transgene in place of *mCherry*. This modular design therefore makes
417 it possible to readily switch between using SyNPL for monitoring and profiling the consequences of
418 defined cell-cell interactions (based on contact-dependent mCherry expression) and using SyNPL for
419 engineering contact-dependent cell behaviours (based on contact-dependent expression of any cell
420 behaviour-determinant).

421 **Describing the properties of the SyNPL system**

422 We characterised various aspects of the SyNPL system that will help inform the experimental design
423 for users of these cells.

424 Previous studies have co-cultured senders and receiver cells at different ratios (ranging from 1:50 to
425 5:1), and for varying times (ranging from 10 minutes to several days) (Cho et al., 2018; Choe et al.,
426 2021; He et al., 2017; Huang et al., 2020; Luo et al., 2019; Matsunaga et al., 2020; Morsut et al., 2016;
427 Roybal et al., 2016; Sgodda et al., 2020; Srivastava et al., 2019; Toda et al., 2018; Toda et al., 2020;
428 Wang et al., 2021; Yang et al., 2020). We analysed transgene induction in STC receiver cells at 11
429 different sender:receiver cell ratios (ranging from 1:19 to 9:1), and observed that higher proportions
430 of sender cells in culture result in a higher proportion of receiver cells inducing mCherry. This is in line
431 with the results obtained by (Sgodda et al., 2020) when comparing three different sender:receiver cell
432 ratios, and with the observations of (Morsut et al., 2016), who exposed receiver cells to varying
433 concentrations of sender ligand. By finely varying the concentrations of sender ligand, Lim and
434 colleagues described the transgene induction response as sigmoidal (Morsut et al., 2016), which was
435 not evident in our data. It is however possible that by testing lower sender:receiver cell ratios this
436 might hold true in our SynNotch system too.

437 When analysing transgene expression within single samples, we found that mCherry distribution
438 follows a bimodal on/off response, indicative of the presence of receiver cells which do not interact
439 with sender cells at low sender:receiver cell ratios. This bimodal pattern of transgene induction is also
440 evident in data from Cantz and colleagues (Sgodda et al., 2020). The ability of individual sender cells
441 to induce mCherry induction in STC receiver cells (as seen in Movies 1 and 3) implies that this system
442 can be effectively employed to study the effect of interactions between receiver cells and individual
443 and/or rare sender cells in relevant model systems.

444 We performed a high-resolution study of the kinetics of mCherry induction and downregulation in STC
445 receiver cells. We observed low levels of mCherry induction in STC receiver cells following 2 hours of
446 co-culture with sender cells, provided we allowed time for subsequent protein maturation, and
447 observed maximum mCherry induction following 48 hours of co-culture. Previous studies making use
448 of lentiviral-delivered transgenes suggest that 10 minutes may be sufficient for transgene activation
449 in HEK293 receiver cells, and that 1 hour may be sufficient for transgene induction in L929 receiver
450 cells, as long as protein maturation time is allowed (Morsut et al., 2016; Sgodda et al., 2020). This is

451 significantly faster than what we observed in this study, and may be ascribable to lentiviral
452 transduction leading to higher levels of SynNotch receptor and/or integration of multiple transgene
453 copies compared to our clonal mouse ESC lines.

454 In our system, mCherry downregulation did not commence for at least 8 hours following simulated
455 loss of sender:receiver cell contact, with full loss of signal occurring after more than 40 hours. This is
456 in line with previous observations in L929 receiver cells, where inducible GFP transgene expression
457 was lost between 24 and 50 hours after sender cells were removed from culture (Morsut et al., 2016).
458 The kinetics of mCherry induction and downregulation suggest that this SynNotch system is suited for
459 the study of cell-cell interactions with a temporal range of hours rather than minutes, and that
460 "memory" of such interactions will persist for a few days. mCherry signal intensity will be influenced
461 not only by the duration of contact but also, where cells have moved apart, by the time elapsed since
462 last contact: this may complicate interpretation of data from this system for some applications. Should
463 this persistence of mCherry signal prove inconvenient for the study of particular processes, the PSNB
464 landing pad parental cell lines can be used to readily generate cell interaction reporter receiver cells
465 harbouring destabilised inducible transgenes with short half-lives.

466 **Exploring the roles of cell-cell interactions *in vivo* and *in vitro***

467 We demonstrated that our clonal mouse ESC lines can be used *in vivo* in chimaeric embryos. The ability
468 to conveniently switch between *in vitro* and *in vivo* experimentation was a key reason for us to
469 establish SynNotch technology in mouse ESCs. Both the receiver lines we generated and the parental
470 PSNB landing pad cell lines offer the power and flexibility to address questions we have so far been
471 unable to answer in *in vitro* and *in vivo* settings. For example, the system could be employed in cell
472 competition studies: STC receiver cells could be used to identify and isolate the direct neighbours of
473 EGFP-tagged "loser" cells, and profiled to study what changes are induced upon interaction with loser
474 cells in order to bring about their elimination. Receiver cells could also be engineered to express
475 candidate fitness-altering transgenes in response to interaction with EGFP-tagged wild-type sender
476 cells, as successfully demonstrated in *Drosophila* by (He et al., 2017).

477 The establishment of this system in mouse ESCs also allows to monitor and manipulate the effects of
478 cell-cell interactions in specific cell types obtained through directed differentiation. We also
479 demonstrated that our cell lines can be used to generate synthetic patterns of gene expression,
480 resulting in spatially-defined programming of cell fate. The combination of directed differentiation of
481 ESCs, spatial confinement of sender and receiver cells, and contact-mediated cell fate engineering
482 provides many possibilities for the study of cell-cell interactions in any developmental process of
483 interest.

484 **Concluding remarks**

485 Cell-cell interactions are a shared feature of the development of all multicellular organisms. Whilst the
486 particulars of these interactions vary greatly amongst eukaryotic supergroups, it is clear that they play
487 an essential role in development (Armingol et al., 2021). The Synthetic Biology field has recently
488 developed several applications to monitor cell communication, such as SynNotch (Morsut et al., 2016)
489 and derivative systems (Zhu et al., 2021), direct transfer of fluorophores to neighbouring cells
490 (Ombrato et al., 2019; Tang et al., 2020), reconstitution of a fluorophore following interaction
491 between different cell types carrying non-fluorescent fluorophore fragments (Kinoshita et al., 2020).
492 We have here demonstrated how SynNotch technology can be used to monitor and manipulate cell-
493 cell interactions in mouse ESCs and in mouse embryos.

494

495 **MATERIALS AND METHODS**

496 **Reagents**

REAGENT	SOURCE	IDENTIFIER	CONCENTRATION
Antibodies and nuclear counterstain			
Mouse monoclonal anti-Flag	Sigma-Aldrich	Cat# F3165; RRID: AB_259529	1:1000
Chicken polyclonal anti-GFP	Abcam	Cat# ab13970; RRID: AB_300798	1:1000
Goat polyclonal anti-Myc	Abcam	Cat# ab9132; RRID: AB_307033	1:1000
Mouse monoclonal anti-Myc AlexaFluor 488 conjugate	Santa Cruz	Cat# sc-40 AF488; RRID: AB_2892598	1:200
Rabbit polyclonal anti-LaminB1	Abcam	Cat#ab16048; RRID: AB_443298	1:1000
Rat monoclonal anti-mCherry	Invitrogen	Cat# M11217; RRID: AB_2536611	1:1000
Mouse monoclonal anti-Nup107 (NPC)	Abcam	Cat# ab24609; RRID: AB_448181	1:1000
Rabbit polyclonal anti-tRFP (tagBFP)	Evrogen	Cat# AB233; RRID: AB_2571743	1:1000
Mouse monoclonal anti-Tubb3	Biolegend	Cat# 801201; RRID: AB_2313773	1:1000
DRAQ7	Abcam	Cat# ab109202	1µM (IF); 300nM (flow cytometry)
DAPI	Biotium	Cat# 40043	1µM
Chemicals and solutions			
2-Mercaptoethanol	Gibco	Cat# 31350010	100nM
Accutase	Sigma-Aldrich	A6964	
Benzyl alcohol	Alfa Aesar	Cat# 100-51-6	
Benzyl benzoate	Sigma	Cat# B9550	
Chorulon (hCG)	Intervet	Cat# CH-475-1	100 IU/ml
DAPT	Abcam	Cat# ab120633	100µM
DMEM, high glucose, no glutamine, no phenol red	Gibco	Cat# 31053028	
Donkey serum	Sigma-Aldrich	Cat# D9663	3% v/v
Doxycycline hyclate	Sigma-Aldrich	Cat# D9891	1µg/ml
Dulbecco's phosphate buffered saline (PBS)	Sigma-Aldrich	Cat# D8537	
Fibronectin from bovine plasma solution	Sigma-Aldrich	Cat# F1141	

Foetal calf serum	Life Technologies	Cat# 10270106	10% v/v
Formaldehyde 37-41%	Fisher Scientific	Cat# F/1501/PB08	4% w/v
Gelatin	Sigma-Aldrich	Cat# G1890	0.1% w/v
Geneticin (G418)	Gibco	Cat# 11811031	200µg/ml
Glasgow Minimum Essential Medium	Sigma-Aldrich	Cat# G5154	
Hygromycin B	Gibco	Cat# 10687010	200µg/ml
L-Glutamine	Thermo Scientific	Cat# 25030024	2mM
Lipofectamine 3000 transfection reagent	Life Technologies	Cat# L3000008	
M2 medium	Sigma-Aldrich	Cat# M7167	
MEM Non-essential amino acids solution (100X)	Gibco	Cat# 11140050	1X
Penicillin/streptomycin	Gibco	Cat# 15140122	100 U/ml
PMSG	ProSpec	Cat# HOR-272	100 IU/ml
Prolong Gold Antifade Mountant	Thermo Fisher	Cat# P36930	
Puromycin dihydrochloride	Sigma-Aldrich	Cat# P8833	2µg/ml
Sodium pyruvate	Gibco	Cat# 11360039	1 mM
Triton X-100	Sigma-Aldrich	Cat# X100	0.1% v/v
Trypsin EDTA 0.25%	Gibco	Cat# 25200072	0.05% w/v
Tyrode's solution, acidic	Sigma-Aldrich	Cat# T1788	
Zeocin	Gibco	Cat# R25001	100µg/ml
Cell culture substrates and inserts			
3 well silicone culture insert	Ibidi	Cat# 80369	
µ-Slide 8 Well	Ibidi	Cat# 80826	
µ-Slide 4 Well	Ibidi	Cat# 80426	
µ-Plate 96 Well Black	Ibidi	Cat# 89626	
µ-Slide Angiogenesis, uncoated	Ibidi	Cat# 81501	
Glass coverslip, 24mm diameter	VWR	Cat# 631-1583	
Plastic flasks and plates for routine cell culture	Corning	Various	
DNA constructs			
pHR_EGFPligand	(Morsut et al., 2016)	Addgene 79129	
pHR_SFFV_LaG17_synNotch_TetRVP64	(Morsut et al., 2016)	Addgene 79128	
pDisplay-EGFP-TM	(Han et al., 2004)		
pHR_TRE-mCherry-PGK-tagBFP-WPRE	Elise Cachat, University of Edinburgh		
CAG-ϕC31 integrase	(Monetti et al., 2011)	Similar plasmid available: Addgene 62658	
pRosa26-DEST-1lox	(Tosti et al., 2018)		
pENTR-2xAttP50	(Tosti et al., 2018)		

pENTR-2xAttB53	(Tosti et al., 2018)		
pPyCAG-EGFP-TM-IRES-Pac	This study	Addgene 183603	
pPyPGK-EGFP-TM-IRES-Pac	This study	Addgene 183604	
pPyCAG-HA-EGFP-Myc-TM-IRES-Pac	This study	Addgene 183605	
pPyPGK-HA-EGFP-Myc-TM-IRES-Pac	This study	Addgene 183606	
pPyPGK-Myc-LaG17-Notch1TM-tTA-IRES-Ble	This study	Addgene 183607	
pPyCAG-tagBFP-3xNLS-IRES-Hph	This study	Addgene 183608	
pmROSA26-attP50-Neo-mKate2-3xNLS-attP50	This study	Addgene 183609	
attB53-Pac-attB53	This study	Addgene 183610	
attB53-Pac-TRE-mCherry-attB53	This study	Addgene 183611	
attB53-Pac-tetO-mCherry-attB53	This study	Addgene 183612	
attB53-Pac-TRE-3xFlag-Neurog1-attB53	This study	Addgene 183613	
attB53_SNCB+_attB53	This study	Addgene 183614	
attB53_SNCB-_attB53	This study	Addgene 183615	
Cell lines			
E14Ju09 mouse ESCs (129/Ola, male)	(Hamilton and Brickman, 2014)		
CmGP1 sender mouse ESCs (129/Ola, male)	This study		
CHmGMP19 sender mouse ESCs (129/Ola, male)	This study		
CmGP1GH1 sender mouse ESCs (129/Ola, male)	This study		
E14GIP1 mouse ESCs (129/Ola, male)	This study		
EM35 mouse ESCs (129/Ola, male)	This study		
SNCB+ receiver mouse ESCs (129/Ola, male)	This study		
SNCB- receiver mouse ESCs (129/Ola, male)	This study		
35SRZ mouse ESCs (129/Ola, male)	This study		
PSNB mouse ESCs (129/Ola, male)			
PSNB-E mouse ESCs (129/Ola, male)	This study		
PSNB-tetO receiver mouse ESCs (129/Ola, male)	This study		
STC receiver mouse ESCs (129/Ola, male)	This study		
STN receiver mouse ESCs (129/Ola, male)	This study		

Animal care and use

Animal experiments were performed under the UK Home Office project license PEEC9E359, approved by the Animal Welfare and Ethical Review Panel of the University of Edinburgh and within the conditions of the Animals (Scientific Procedures) Act 1986.

Chimaera generation

503 C57BL/6 female mice (Charles River) were superovulated (100 IU/ml PMSG and 100 IU/ml hCG
504 intraperitoneal injections 48 hours apart) and crossed with wild-type stud male mice. Pregnant mice
505 were culled at embryonic day 2.5 (E2.5) by cervical dislocation, ovaries with oviducts were dissected
506 and collected in pre-warmed M2 medium. Oviducts were flushed using PBS and a 20-gauge needle
507 attached to a 1ml syringe and filled with PB1 (Whittingham, 1974). E2.5 embryos were collected and
508 washed in PB1, their zona pellucida was removed using acidic Tyrode's solution, and they were
509 transferred to a plate with incisions where two clumps of approximately 8 sender and 8 receiver cells
510 were added to each embryo. Embryos were then incubated at 37°C in 5% CO_2 for 48 hours prior to
511 fixation, or for 24 hours prior to transfer to pseudopregnant females for the generation of post-
512 implantation chimaeras. For DAPT treatment experiments, DAPT was equilibrated for several hours at
513 37°C prior to addition to embryos in order to avoid precipitation. Embryos subject to DAPT withdrawal
514 were washed twice before being placed in DAPT-free medium. The sex of embryos used in this study
515 was not determined.

516 **Mouse ESC culture**

517 Mouse embryonic stem cells were routinely maintained on gelatinised culture vessels (Corning) at
518 37°C and 5% CO_2 in Glasgow Minimum Essential Medium (GMEM) supplemented with 10% foetal calf
519 serum (FCS), 100U/ml LIF (produced in-house), 100nM 2-mercaptoethanol, 1X non-essential amino
520 acids, 2mM L-Glutamine), 1mM Sodium Pyruvate (medium referred to as "ES cell culture medium" or
521 "LIF+FCS"). The medium was supplemented with 200µg/ml G418, 2µg/ml puromycin, 200µg/ml
522 hygromycin B and/or 100µg/ml zeocin as appropriate.
523 For live imaging, GMEM was replaced with phenol red-free Dulbecco's Modified Eagle Medium
524 (DMEM), with all other components of the culture medium used at identical concentrations.

525 **DNA constructs**

526 pHR_SFFV_LaG17_synNotch_TetRVP64 (Addgene plasmid #79128) (Morsut et al., 2016) and
527 pHR_EGFPligand (Addgene plasmid #79129) (Morsut et al., 2016) were kind gifts from Dr Wendell Lim
528 (UCSF) and Dr Leonardo Morsut (USC). pDisplay-GFP-TM (Han et al., 2004) was a kind gift of Dr Luis
529 Ángel Fernández (CNB-CSIC). CAG-ϕC31 integrase (Monetti et al., 2011) was a kind gift of Dr Andras
530 Nagy (Lunenfeld-Tanenbaum Research Institute). pHR_TRE-mCherry-PGK-tagBFP-WPRE was a kind
531 gift of Dr Elise Cachat (The University of Edinburgh). pRosa26-DEST-1lox, pENTR-2xAttP50 and pENTR-
532 2xAttB53 (Tosti et al., 2018) constructs were kind gifts of Dr Keisuke Kaji (The University of Edinburgh).

533 Untagged transmembrane EGFP constructs were generated by digesting pHR_EGFPligand with
534 XhoI+NotI, and ligating the *IgGK signal-EGFP-PDGFRB TMD* cassette into XhoI+NotI-digested *pPyCAG-*
535 *IRES-Pac* (Malaguti et al., 2019) or *pPyPGK-IRES-Pac* (Rao et al., 2020) vector backbones. HA- and Myc-
536 tagged EGFP constructs were generated by PCR-amplifying an *IgGK signal-HA-EGFP-Myc-PDGFRB TMD*
537 cassette flanked by PspXI and NotI sites from pDisplay-GFP-TM, digesting the amplicon with
538 PspXI+NotI, and ligating the insert into XhoI+NotI-digested *pPyCAG-IRES-Pac* or *pPyPGK-IRES-Pac*
539 vector backbones.

540 The *pPyPGK-CD8a signal-Myc-LaG17-Notch1 minimal transmembrane core-tTA-IRES-Ble* SynNotch
541 receptor construct was generated by PCR-amplifying a *CD8a signal-Myc-LaG17-Notch1 minimal*
542 *transmembrane core-tTA* cassette flanked by XhoI and Bsu36I sites from
543 pHR_SFFV_LaG17_synNotch_TetRVP64, digesting the amplicon with XhoI+Bsu36I, and ligating the
544 insert into a XhoI+Bsu36I-digested *pPyPGK-IRES-Ble* vector backbone. The mouse Notch1 minimal
545 transmembrane core consists of residues 1427-1752 (Uniprot: Q01705).

546 The *pPyCAG-tagBFP-3xNLS-IRES-Hph* construct was generated by PCR-amplifying a *tagBFP* cassette
547 flanked by XhoI and KasI sites from pHR_TRE-mCherry-PGK-tagBFP-WPRE, digesting the amplicon with
548 XhoI+KasI, and ligating the insert into a XhoI+NotI-digested *pPyCAG-IRES-Hph* backbone (Malaguti et
549 al., 2019) alongside oligonucleotides annealed to generate a *3xNLS* fragment with KasI and NotI
550 overhangs (Malaguti et al., 2013).

551 The *Rosa26* landing pad targeting vector was generated by Gateway Cloning (Invitrogen) of an *attL1-*
552 *attP50-Neo-SV40pA-(CAG-mKate2-3xNLS-bGHpA)-attP50-attL2* cassette into the pRosa26-DEST-1lox
553 targeting vector. Its final structure is as follows: *Rosa26 5'HA-splice acceptor-loxP-attP50-Neo-*
554 *SV40pA-(CAG-mKate2-3xNLS-bGHpA)-attP50-Rosa26 3'HA-PGK-DTA-bGHpA*. Sequence in brackets is
555 on -strand.

556 An *attB53-Pac-attB53* "empty vector" construct for RMCE at the *Rosa26* locus was generated by
557 adding a *Pac-bGHpA* cassette followed by an EcoRV restriction site to pENTR-2xAttB53 by Gibson
558 assembly.
559 The attB53-TRE-mCherry-attB53 RMCE construct used to generated STC receiver cells from PSNB
560 landing pad lines was generated by PCR-amplifying a *TRE-mCherry-SV40pA* cassette flanked by EcoRV-
561 AscI and EcoRV-BamHI sites from pHR_TRE-mCherry-PGK-tagBFP-WPRE, digesting the amplicon with
562 EcoRV, ligating the insert into EcoRV-digested *attB53-Pac-attB53* backbone, and screening for
563 insertion on the -strand. The attB53-tetO-mCherry-attB53 RMCE construct used to generate PSNB-
564 tetO cells from PNSB landing pad lines was generated by PCR-amplifying a *tetO-mCherry-rBGpA*
565 cassette flanked by MluI and BamHI sites, digesting the amplicon with MluI+BamHI and ligating the
566 insert into AscI+BamHI-digested *attB53-Pac-TRE-mCherry-attB53*.
567 The attB53-TRE-3xFlag-Neurog1-attB53 RMCE construct used to generate STN receiver cells from
568 PSNB landing pad lines was generated by PCR-amplifying a *3xFlag-Neurog1* cassette flanked by NdeI
569 and MfeI sites from wild-type mouse cDNA, digesting the amplicon with NdeI+MfeI and ligating the
570 insert into NdeI+MfeI-digested *attB53-Pac-TRE-mCherry-attB53* backbone (in which *mCherry* is
571 flanked by NfeI and MfeI sites).

572 attB53_SNCB+_attB53 and attB53_SNCB_attB53 constructs were generated in two steps. First, the
573 base *attB53-Pac-bGHpA-attB53* RMCE construct was linearised with EcoRV, and ligated with a HincII-
574 *PGK-CD8a signal-Myc-LaG17-Notch1 minimal transmembrane core-tTA*-HindIII fragment (digested
575 from the SynNotch receptor construct described above) and a HindIII-*bGHpA*-EcoRV fragment, and
576 clones were screened for insertion of the SynNotch receptor on the +strand. Next, the resulting
577 construct was linearised with EcoRV, and ligated with an EcoRV-*TRE-mCherry-SV40pA-PGK-tagBFP-*
578 PacI fragment (digested from pHR_TRE-mCherry-PGK-tagBFP-WPRE) and a PacI-*bGHpA*-EcoRV
579 fragment. Correct assembly on the + and - strands generated the attB53_SNCB+_attB53and
580 attB53_SNCB-_attB53 constructs respectively.

581 Abbreviations: TMD: transmembrane domain; IRES: internal ribosome entry site; 5'/3' HA: 5'/3'
582 homology arm; SV40pA: SV40 polyadenylation signal sequence; bGHpA: bovine growth hormone
583 polyadenylation signal sequence; rBGpA: rabbit beta-globin polyadenylation signal sequence; NLS:
584 nuclear localisation signal; PGK: mouse *Pgk1* promoter; Pac: puromycin N-acetyltransferase; Hph:
585 hygromycin B phosphotransferase; Ble: bleomycin resistance gene (confers zeocin resistance); tTA:
586 tetracycline transactivator.

587 Plasmids that we generated for this study will be made available on Addgene.

588 **Transfections**

589 For electroporations, 10^7 ESCs were electroporated with 100µg DNA using a BioRad GenePulser set to
590 800V/3µF. For nucleofections, $5x10^5$ ESCs were nucleofected with 5µg DNA with the Lonza P3 Primary
591 Cell Nucleofector Unit and kit, using program CG-104, and following manufacturer instructions. For
592 lipofections, 10^5 ESCs were lipofected with 3µg DNA mixed with 3µl Lipofectamine 3000 and 6µl P3000
593 solution, following manufacturer instructions. For ϕC31-mediated RMCE, equal masses of RMCE
594 constructs and CAG-ϕC31 vector were transfected.
595 Clonal ESC lines were generated by transfecting constructs of interest into ESCs, then plating cells at
596 low density onto gelatinised 9cm dishes in the absence of selection. Selective medium was added 48
597 hours post-transfection and replaced every other day. After 7-10 days, clones were manually picked,
598 dissociated, and replated into gelatinised 96-well culture plates. Clones were transferred to
599 gelatinised vessels with larger culture areas when confluent, screened as appropriate, expanded and
600 cryopreserved.

601 **Cell lines**

602 E14Ju09 ESCs are a 129/Ola male wild-type clonal line derived from E14tg2a (Hamilton and Brickman,
603 2014; Hooper et al., 1987).
604 Sender cells were generated by electroporating E14Ju09 ESCs with one of four constructs: *pPyCAG-*
605 *IgGK signal-EGFP-PDGFRB TMD-IRES-Pac* (CmGP cells), *pPyPGK-IgGK signal-EGFP-PDGFRB TMD-IRES-*
606 *Pac* (PmGP cells), *pPyCAG-IgGK signal-HA-EGFP-Myc-PDGFRB TMD-IRES-Pac* (CHmGMP cells),
607 *pPyPGK-IgGK signal-HA-EGFP-Myc-PDGFRB TMD-IRES-Pac* (PHmGMP cells). Simplified versions of the
608 constructs are displayed in Fig. 2. HA and Myc tags were used in CHmGMP and PHmGMP cell lines as
609 additional markers to identify sender cells, but are not essential given that sender cells can be
610 identified by GFP fluorescence. CmGP1GH1 sender cells were generated by lipofecting CmGP1 sender
611 cells with a *pPyCAG-EGFP-IRES-Hph* construct. E14GIP1 "cytoplasmic sender" cells were generated by
612 lipofecting E14Ju09 ESCs with a *pPyCAG-EGFP-IRES-Pac* construct.
613 EM35 landing pad cells were generated by electroporating E14Ju09 ESCs with the *Rosa26* landing pad
614 targeting vector described above. Correct targeting was verified by genomic DNA PCR with the
615 following primers: Forward: GGCGGACTGGCGGGACTA, Reverse:
616 GGGACAGGATAAGTATGACATCATCAAGG. Primer locations and expected band sizes are displayed in
617 Fig. S3A. This PCR strategy was modified from that described by (Mort et al., 2014) to suit the different
618 sequence of our *Rosa26* targeting vector.
619 SNCB+ and SNCB- receiver cells were generated by electroporating EM35 ESCs with the constructs
620 depicted in Figs. S4A, S6A, and a *CAG-φC31 integrase* construct to mediate RMCE.
621 35SRZ landing pad cells were generated by electroporating EM35 landing pad cells with *pPyPGK-CD8a*
622 *signal-Myc-LaG17-Notch1 minimal transmembrane core-tTA-IRES-Ble*.
623 PSNB landing pad cell lines were generated by nucleofecting 35SRZ ESCs with a *pPyCAG-tagBFP-3xNLS-*
624 *IRES-Hph* construct. PSNB-A cells were derived from 35SRZ clone 9 (PSNB-A clone 10 renamed PSNB
625 clone A), PSNB-B cells were derived from 35SRZ clone 86 (PNSB-B clone 3 renamed PSNB clone B).
626 STC receiver cells were generated by nucleofecting PSNB ESCs with *CAG-φC31 integrase* and the
627 following RMCE construct: *attB53-Pac-bGHpA-(TRE-mCherry-SV40pA)-attB53*. Sequence in brackets is
628 on -strand. STC clone A1 was derived from PSNB clone A, STC clones B1 and B2 were derived from
629 PSNB clone B.
630 PSNB-tetO cells were generated by nucleofecting PSNB ESCs with *CAG-φC31 integrase* and the
631 following RMCE construct: *attB53-Pac-bGHpA-(tetO-mCherry-SV40pA)-attB53*. Sequence in brackets
632 is on -strand.
633 PNSB-E cells were generated by nucleofecting PSNB ESCs with *CAG-φC31 integrase* and the following
634 RMCE construct: *attB53-Pac-bGHpA-attB53*.

635 STN receiver cells were generated by nucleofecting PSNB clone A ESCs with *CAG-φC31 integrase* and
636 the following RMCE construct: *attB53-Pac-bGHpA-(TRE-3xFlag-Neurog1-SV40pA)-attB53*. Sequence in
637 brackets is on -strand.

638 Cell lines generated in this study were routinely karyotyped by chromosome count, checked for
639 absence of mycoplasma infection, and are available on request.

640 **Co-culture experiments**

641 Sender and receiver cells were detached from culture vessels with accutase, quenched in ESC culture
642 medium, pelleted by spinning at 300g for 3 minutes, resuspended in ESC culture medium
643 supplemented with 2µg/ml puromycin and counted. Cells were plated at ratios described in figure
644 legends, and at empirically determined optimal densities.
645 For flow cytometry experiments, cells were plated onto 12-well plates coated with 7.5µg/ml
646 fibronectin, at the following densities: experiments carried out in the absence of doxycyline: 1h-8h:
647 $4x10^5$ cells/well; 16h: $2.4x10^5$ cells/well; 24h: $1.6x10^5$ cells/well; 48h: $8x10^4$ cells/well; 72h: $4x10^4$
648 cells/well. mCherry induction with 16h doxycycline (Fig. 4F-H): 0-4h: $2.4x10^5$ cells/well; 5-8h: $1.6x10^5$
649 cells/well; 24h: $8x10^4$ cells/well. mCherry downregulation experiments (Fig. S14): 0h-8h: $1.6x10^5$
650 cells/well; 16h: $1.2x10^5$ cells/well; 24h: $8x10^4$ cells/well; 48h: $4x10^4$ cells/well.
651 For immunofluorescence experiments, cells were plated on flamed 24mm glass coverslips housed in
652 a 6-well plate coated with 7.5µg/ml fibronectin.
653 For live imaging experiments using a Nikon Ti-E microscope (Movies 1,3-5), cells were plated onto an
654 8-well imaging slide coated with 7.5µg/ml fibronectin, at the following densities: mCherry induction
655 experiments: $3x10^4$ cells/well; mCherry downregulation experiments: 0-24h: $2x10^4$ cells/well; 24-48h:
656 10^4 cells/well. For live imaging experiments using a PerkinElmer Opera Phenix Plus microscope (Movie
657 2, Fig. S16G), cells were plated onto a 96-well imaging plate coated with 7.5µg/ml fibronectin, at the
658 following densities: mCherry induction experiments: $9.6x10^4$ cells/well; mCherry downregulation
659 experiments: 0-24h: $2x10^4$ cells/well; 24-48h: 10^4 cells/well. ESC culture medium was supplemented
660 with 2µg/ml puromycin, 200µg/ml hygromycin B and 1X penicillin/streptomycin.
661 To test induction of 3xFlag-Neurog1 in STN receiver cells, CmGP1 sender cells and STN receiver cells
662 were plated at a 9:1 ratio at a concentration of $2x10^5$ cells/well onto a 24mm flamed glass coverslip
663 housed in a 6-well plate coated with 7.5µg/ml fibronectin, then fixed and stained after 48 hours.

664 **Synthetic patterning experiments**

665 A 24mm glass coverslip housed in a 6-well plate was coated with 7.5µg/ml fibronectin, then allowed
666 to air dry. When fully dry, forceps were used to place a culture insert 3-well silicon chamber on top of
667 the coverslip; downward force was carefully exerted to secure it in place. $4x10^4$ cells were plated
668 overnight in 70µl culture medium in each of the three wells. Sender cells were plated in the central
669 well, and receiver cells were plated in the outside wells. 2ml culture medium were added outside of
670 the 3-well insert in order to prevent evaporation. The next day, the 2ml culture medium outside of
671 the 3-well insert were aspirated, and the 70µl in each of the three wells were carefully removed in
672 order not to dislodge the 3-well insert. Each well was quickly washed with 70µl PBS to get rid of any
673 remaining cells in suspension. Forceps were used to detach the 3-well insert from the glass coverslip,
674 and 2.5ml culture medium were added to the well. Culture medium was replaced daily. Growth of
675 cells into the gaps between wells were monitored daily; following contact between sender and
676 receiver cells, cells were kept in culture for a further 24 hours (STC receivers + CmGP1 senders) or a
677 further 96 hours (STN receivers + CmGP1 senders) prior to fixation and immunofluorescence. For live
678 imaging of mCherry stripe experiments, the 3-well insert was placed in an Ibidi µ-Slide 4 Well instead
679 of on a glass coverslip.

680 **Flow cytometry**

681 Cells were washed in PBS, then detached from culture vessels with accutase. They were resuspended
682 in ice-cold PBS+10% FCS, pelleted by spinning at 300g for 3 minutes, resuspended in ice-cold PBS+10%
683 FCS+300nM DRAQ7 and placed on ice before analysing on a BD LSRFortessa flow cytometer. Forward
684 and side-scatter width and amplitude were used to identify single cells in suspension, dead cells were
685 excluded by gating on DRAQ7-negative cells, and tagBFP, GFP and mCherry/mKate2 expression were
686 then analysed using V 450/50-A, B 530/30-A, Y/G 610/20-A laser/filters combinations respectively.

687 **Immunofluorescence**

688 Cells were plated on flamed glass coverslips coated with 7.5µg/ml fibronectin and cultured as
689 indicated in figure legends. Cells were washed with PBS, fixed in 4% formaldehyde in PBS for 20
690 minutes at room temperature, then washed three times in PBS for a total of 15 minutes. Cells were
691 blocked overnight at 4°C in blocking solution (PBS+3% donkey serum+0.1% Triton X-100). Primary
692 antibodies diluted in blocking solution were added for 3 hours at room temperature, the coverslips
693 were washed 3 times in PBS for a total of 30 minutes, secondary antibodies diluted in blocking solution
694 were added for 1 hour at room temperature, the coverslips were washed 3 times in PBS for a total of
695 30 minutes. The coverslips were then mounted onto glass slides in Prolong Gold mounting medium.
696 For synthetic patterning experiments and chimaera stainings, antibodies were incubated overnight at
697 4°C or 37°C respectively to improve penetration. Blastocysts were imaged in PBS in an imaging
698 chamber, and scoring of mCherry-HI cells was performed manually using chimaeras containing both
699 sender and receiver cells as a reference. Post-implantation chimaeras were were dehydrated in
700 methanol series in PBS/0.1% Triton X-100, clarified in 50% methanol/50% BABB (benzyl alcohol:benzyl
701 benzoate 1:2 ratio), and transferred into 100% BABB before imaging. All imaging was performed on a
702 Leica SP8 confocal microscope with a 40X immersion lens unless otherwise indicated.

703 **Live imaging**

704 Cells to be imaged were allowed to adhere on culture vessels at room temperature for 15 minutes
705 after plating, after which they were placed in a 37°C 5% CO_2 humidified chamber and imaged. For
706 Movies 1, 3-5, imaging was performed with a widefield Nikon Ti-E microscope, 20X lens, and
707 Hamamatsu camera; images were taken at 10-minute intervals for 24 hours, and xy coordinates were
708 saved. Following live imaging, cells were fixed and stained for fluorophore expression, and imaged at
709 the previously saved xy coordinates (Movies 1,3). For Movie 2, Fig. S16G and Fig. S19, imaging was
710 performed with a PerkinElmer Opera PhenixPlus microscope, 20X lens. Images were taken at 1-hour
711 (Movie 2, Fig. S16G) or 90-minute (Fig. S19) intervals for 24 hours. Fully automated segmentation of
712 tagBFP-positive nuclei, tracking, and quantification of fluorescent signal intensity in live imaging
713 experiments was performed using the PerkinElmer Harmony software.

714 Filming of the morula to blastocyst transition was performed with a PerkinElmer Opera PhenixPlus
715 confocal microscope. Sender and receiver cells were placed on opposite poles of morulae, and allowed
716 to aggregate unperturbed for approximately 4 hours prior to imaging, in order to ensure strong
717 binding of ES cells to morulae. They were then transferred to wells of an uncoated Ibidi µ-Slide
718 Angiogenesis imaging slide and imaged. Aside from an initial frame, it was not possible to capture
719 tagBFP signal within the time-lapse movies as embryos were vulnerable to repeated stimulation with
720 ultraviolet light.

721

722 **ACKNOWLEDGEMENTS**

We thank Leonardo Morsut and Wendell Lim for developing the original SynNotch system, Elise Cachat and Keisuke Kaji for advice and reagents, Luis Ángel Fernández for the pDisplay-EGFP-TM plasmid, Andras Nagy for the CAG-ϕC31 plasmid, Dónal O'Carroll and Pedro Moreira for assistance with generating chimaeric mice, Eve Moutaux for cloning initial versions of the RMCE constructs, Alexandre Veiga and Matthew French for performing preliminary experiments with the original SynNotch constructs. We thank Justyna Cholewa-Waclaw, Matthieu Vermeren and Charles Williams for assistance with time-lapse imaging, Fiona Rossi and Claire Cryer for flow cytometry support, and Theresa O'Connor, Helen Henderson and Marilyn Thomson for cell culture support. We are grateful to Leonardo Morsut and members of the Lowell and Wilson labs for helpful discussions.

COMPETING INTERESTS

The authors declare no competing interests.

FUNDING

This work was funded by a Wellcome Trust Senior Fellowship to SL (WT103789AIA) and a Wellcome Trust Sir Henry Wellcome Fellowship to GB (WT100133).

REFERENCES

Armingol, E., Officer, A., Harismendy, O. and Lewis, N. E. (2021). Deciphering cell–cell interactions and communication from gene expression. *Nature Reviews Genetics* **22**, 71–88.

Arnold, S. J. and Robertson, E. J. (2009). Making a commitment: cell lineage allocation and axis patterning in the early mouse embryo. *Nature Reviews Molecular Cell Biology* **10**, 91–103.

Blin, G., Wisniewski, D., Picart, C., Thery, M., Puceat, M. and Lowell, S. (2018). Geometrical confinement controls the asymmetric patterning of Brachyury in cultures of pluripotent cells. *Development*.

Blin, G., Sadurska, D., Migueles, R. P., Chen, N., Watson, J. A. and Lowell, S. (2019). Nessys: A new set of tools for the automated detection of nuclei within intact tissues and dense 3D cultures. *PLOS Biol.* **17**, e3000388.

Boggs, S. S., Gregg, R. G., Borenstein, N. and Smithies, O. (1986). Efficient transformation and frequent single-site, single-copy insertion of DNA can be obtained in mouse erythroleukemia cells transformed by electroporation. *Experimental Hematology* **14**, 988–994.

Bradley, A., Evans, M., Kaufman, M. H. and Robertson, E. (1984). Formation of germ-line chimaeras from embryo-derived teratocarcinoma cell lines. *Nature* **309**, 255–256.

Cachat, E., Liu, W., Martin, K. C., Yuan, X., Yin, H., Hohenstein, P. and Davies, J. A. (2016). 2- and 3-dimensional synthetic large-scale de novo patterning by mammalian cells through phase separation. *Sci. Rep.* **6**, 20664.

760 **Cai, L., Morrow, E. M. and Cepko, C. L.** (2000). Misexpression of basic helix-loop-helix genes in the
761 murine cerebral cortex affects cell fate choices and neuronal survival. *Development* **127**,
762 3021–3030.

763 **Cau, E., Casarosa, S. and Guillemot, F.** (2002). Mash1 and Ngn1 control distinct steps of
764 determination and differentiation in the olfactory sensory neuron lineage. *Development* **129**,
765 1871–1880.

766 **Charrier, S., Ferrand, M., Zerbato, M., Précigout, G., Viornery, A., Bucher-Laurent, S., Benkhelifa-**
767 **Ziyyat, S., Merten, O. W., Perea, J. and Galy, A.** (2011). Quantification of lentiviral vector
768 copy numbers in individual hematopoietic colony-forming cells shows vector dose-
769 dependent effects on the frequency and level of transduction. *Gene Therapy* **18**, 479–487.

770 **Chen, C., Krohn, J., Bhattacharya, S. and Davies, B.** (2011). A Comparison of Exogenous Promoter
771 Activity at the ROSA26 Locus Using a PhiC31 Integrase Mediated Cassette Exchange
772 Approach in Mouse ES Cells. *PLOS ONE* **6**, e23376.

773 **Cho, J. H., Okuma, A., Al-Rubaye, D., Intisar, E., Junghans, R. P. and Wong, W. W.** (2018).
774 Engineering Axl specific CAR and SynNotch receptor for cancer therapy. *Scientific Reports* **8**,
775 3846.

776 **Choe, J. H., Watchmaker, P. B., Simic, M. S., Gilbert, R. D., Li, A. W., Krasnow, N. A., Downey, K. M.,**
777 **Yu, W., Carrera, D. A., Celli, A., et al.** (2021). SynNotch-CAR T cells overcome challenges of
778 specificity, heterogeneity, and persistence in treating glioblastoma. *Sci Transl Med* **13**,.

779 **Davies, J.** (2017). Using synthetic biology to explore principles of development. *Development* **144**,
780 1146–1158.

781 **De Los Angeles, A., Ferrari, F., Xi, R., Fujiwara, Y., Benvenisty, N., Deng, H., Hochedlinger, K.,**
782 **Jaenisch, R., Lee, S., Leitch, H. G., et al.** (2015). Hallmarks of pluripotency. *Nature* **525**, 469–
783 478.

784 **Dias, A. S., Almeida, I. de, Belmonte, J. M., Glazier, J. A. and Stern, C. D.** (2014). Somites Without a
785 Clock. *Science* **343**, 791–795.

786 **Ebrahimkhani, M. R. and Ebisuya, M.** (2019). Synthetic developmental biology: build and control
787 multicellular systems. *Curr. Opin. Chem. Biol.* **52**, 9–15.

788 **Evans, M. J. and Kaufman, M. H.** (1981). Establishment in culture of pluripotential cells from mouse
789 embryos. *Nature* **292**, 154–156.

790 **Fischer, S. C., Corujo-Simon, E., Lilao-Garzon, J., Stelzer, E. H. K. and Muñoz-Descalzo, S.** (2020). The
791 transition from local to global patterns governs the differentiation of mouse blastocysts.
792 *PLOS ONE* **15**, e0233030.

793 **Forsyth, J. E., Al-Anbaki, A. H., Fuente, R. de la, Modare, N., Perez-Cortes, D., Rivera, I., Kelly, R. S.,**
794 **Cotter, S. and Plusa, B.** (2021). IVEN: A quantitative tool to describe 3D cell position and
795 neighbourhood reveals architectural changes in FGF4-treated preimplantation embryos.
796 *PLOS Biology* **19**, e3001345.

797 **Fridy, P. C., Li, Y., Keegan, S., Thompson, M. K., Nudelman, I., Scheid, J. F., Oeffinger, M.,**
798 **Nussenzweig, M. C., Fenyö, D., Chait, B. T., et al.** (2014). A robust pipeline for rapid
799 production of versatile nanobody repertoires. *Nature Methods* **11**, 1253–1260.

800 **Friedrich, G. and Soriano, P.** (1991). Promoter traps in embryonic stem cells: a genetic screen to
801 identify and mutate developmental genes in mice. *Gene Dev* **5**, 1513–1523.

802 **Gorfinkiel, N. and Martinez Arias, A.** (2021). The cell in the age of the genomic revolution: Cell
803 Regulatory Networks. *Cells & Development* 203720.

804 **Gossen, M. and Bujard, H.** (1992). Tight control of gene expression in mammalian cells by
805 tetracycline-responsive promoters. *Proceedings of the National Academy of Sciences* **89**,
806 5547–5551.

807 **Gurdon, J. B.** (1987). Embryonic induction — molecular prospects. *Development* **99**, 285–306.

808 **Hamilton, W. B. and Brickman, J. M.** (2014). Erk signaling suppresses embryonic stem cell self-
809 renewal to specify endoderm. *Cell Reports* **9**, 2056–2070.

810 **Han, H.-J., Park, S.-G., Kim, S.-H., Hwang, S.-Y., Han, J., Traicoff, J., Kho, W.-G. and Chung, J.-Y.**
811 (2004). Epidermal growth factor-like motifs 1 and 2 of Plasmodium vivax merozoite surface
812 protein 1 are critical domains in erythrocyte invasion. *Biochemical and Biophysical Research*
813 *Communications* **320**, 563–570.

814 **He, L., Huang, J. and Perrimon, N.** (2017). Development of an optimized synthetic Notch receptor as
815 an in vivo cell–cell contact sensor. *Proc. Natl. Acad. Sci.* **114**, 5467–5472.

816 **Herbst, F., Ball, C. R., Tuorto, F., Nowrouzi, A., Wang, W., Zavidij, O., Dieter, S. M., Fessler, S.,**
817 **Hoeven, F. van der, Kloz, U., et al.** (2012). Extensive Methylation of Promoter Sequences
818 Silences Lentiviral Transgene Expression During Stem Cell Differentiation In Vivo. *Molecular*
819 *Therapy* **20**, 1014–1021.

820 **Ho, C. and Morsut, L.** (2021). Novel synthetic biology approaches for developmental systems. *Stem*
821 *Cell Reports* **16**, 1051–1064.

822 **Hong, S., Hwang, D.-Y., Yoon, S., Isacson, O., Ramezani, A., Hawley, R. G. and Kim, K.-S.** (2007).
823 Functional Analysis of Various Promoters in Lentiviral Vectors at Different Stages of In Vitro
824 Differentiation of Mouse Embryonic Stem Cells. *Molecular Therapy* **15**, 1630–1639.

825 **Hooper, M., Hardy, K., Handyside, A., Hunter, S. and Monk, M.** (1987). HPRT-deficient (Lesch–
826 Nyhan) mouse embryos derived from germline colonization by cultured cells. *Nature* **326**,
827 292–295.

828 **Huang, J., Zhou, W., Dong, W., Watson, A. M. and Hong, Y.** (2009). Directed, efficient, and versatile
829 modifications of the Drosophila genome by genomic engineering. *Proceedings of the*
830 *National Academy of Sciences* **106**, 8284–8289.

831 **Huang, H., Zhang, X., Lv, J., Yang, H., Wang, X., Ma, S., Shao, R., Peng, X., Lin, Y. and Rong, Z.**
832 (2020). Cell-cell contact-induced gene editing/activation in mammalian cells using a
833 synNotch-CRISPR/Cas9 system. *Protein & Cell* **11**, 299–303.

834 **Johnson, M. H. and Ziomek, C. A.** (1983). Cell interactions influence the fate of mouse blastomeres
835 undergoing the transition from the 16- to the 32-cell stage. *Developmental Biology* **95**, 211–
836 218.

837 **Kinoshita, M. and Smith, A.** (2018). Pluripotency Deconstructed. *Development, Growth &*
838 *Differentiation* **60**, 44–52.

839 **Kinoshita, N., Huang, A. J. Y., McHugh, T. J., Miyawaki, A. and Shimogori, T.** (2020). Diffusible
840 GRAPHIC to visualize morphology of cells after specific cell–cell contact. *Scientific Reports* **10**,
841 14437.

842 **Kondoh, G., Gao, X.-H., Nakano, Y., Koike, H., Yamada, S., Okabe, M. and Takeda, J.** (1999). Tissue-
843 inherent fate of GPI revealed by GPI-anchored GFP transgenesis. *FEBS Letters* **458**, 299–303.

844 **Liew, C.-G., Draper, J. S., Walsh, J., Moore, H. and Andrews, P. W.** (2007). Transient and Stable
845 Transgene Expression in Human Embryonic Stem Cells. *Stem Cells* **25**, 1521–1528.

846 **Luo, H., Wu, X., Sun, R., Su, J., Wang, Y., Dong, Y., Shi, B., Sun, Y., Jiang, H. and Li, Z.** (2019). Target-
847 Dependent Expression of IL12 by synNotch Receptor-Engineered NK92 Cells Increases the
848 Antitumor Activities of CAR-T Cells. *Frontiers in Oncology* **9**,.

849 **Ma, Q., Kintner, C. and Anderson, D. J.** (1996). Identification of neurogenin, a Vertebrate Neuronal
850 Determination Gene. *Cell* **87**, 43–52.

851 **Ma, Q., Chen, Z., Barrantes, I. del B., Pompa, J. L. de la and Anderson, D. J.** (1998). neurogenin1 Is
852 Essential for the Determination of Neuronal Precursors for Proximal Cranial Sensory Ganglia.
853 *Neuron* **20**, 469–482.

854 **Malaguti, M., Nistor, P. A., Blin, G., Pegg, A., Zhou, X. and Lowell, S.** (2013). Bone morphogenic
855 protein signalling suppresses differentiation of pluripotent cells by maintaining expression of
856 E-Cadherin. *eLife* **2**, e01197.

857 **Malaguti, M., Migueles, R. P., Blin, G., Lin, C.-Y. and Lowell, S.** (2019). Id1 Stabilizes Epiblast Identity
858 by Sensing Delays in Nodal Activation and Adjusting the Timing of Differentiation. *Dev. Cell*
859 **50**, 462–477.e5.

860 **Martin, G. R.** (1981). Isolation of a pluripotent cell line from early mouse embryos cultured in
861 medium conditioned by teratocarcinoma stem cells. *Proceedings of the National Academy of*
862 *Sciences* **78**, 7634–7638.

863 **Matsuda, M., Koga, M., Woltjen, K., Nishida, E. and Ebisuya, M.** (2015). Synthetic lateral inhibition
864 governs cell-type bifurcation with robust ratios. *Nat Commun* **6**, 6195.

865 **Matsunaga, S., Jeremiah, S. S., Miyakawa, K., Kurotaki, D., Shizukuishi, S., Watashi, K., Nishitsuji,**
866 **H., Kimura, H., Tamura, T., Yamamoto, N., et al.** (2020). Engineering Cellular Biosensors
867 with Customizable Antiviral Responses Targeting Hepatitis B Virus. *iScience* **23**,.

868 **McBurney, M. W., Sutherland, L. C., Adra, C. N., Leclair, B., Rudnicki, M. A. and Jardine, K.** (1991).
869 The mouse Pgk-1 gene promoter contains an upstream activator sequence. *Nucleic Acids*
870 *Research* **19**, 5755–5761.

871 **Monetti, C., Nishino, K., Biechele, S., Zhang, P., Baba, T., Woltjen, K. and Nagy, A.** (2011). PhiC31
872 integrase facilitates genetic approaches combining multiple recombinases. *Methods* **53**,
873 380–385.

874 **Morsut, L., Roybal, K. T., Xiong, X., Gordley, R. M., Coyle, S. M., Thomson, M. and Lim, W. A.**
875 (2016). Engineering Customized Cell Sensing and Response Behaviors Using Synthetic Notch
876 Receptors. *Cell* **164**, 780–791.

877 **Mort, R. L., Ford, M. J., Sakaue-Sawano, A., Lindstrom, N. O., Casadio, A., Douglas, A. T., Keighren,**
878 **M. A., Hohenstein, P., Miyawaki, A. and Jackson, I. J.** (2014). Fucci2a: A bicistronic cell cycle
879 reporter that allows Cre mediated tissue specific expression in mice. *Cell Cycle* **13**, 2681–
880 2696.

881 **Nishida-Aoki, N. and Gujral, T. S.** (2019). Emerging approaches to study cell-cell interactions in
882 tumor microenvironment. *Oncotarget* **10**, 785–797.

883 **Niwa, H., Yamamura, K. and Miyazaki, J.** (1991). Efficient selection for high-expression transfectants
884 with a novel eukaryotic vector. *Gene* **108**, 193–199.

885 **Nowotschin, S. and Hadjantonakis, A.-K.** (2010). Cellular dynamics in the early mouse embryo: from
886 axis formation to gastrulation. *Current Opinion in Genetics & Development* **20**, 420–427.

887 **Nowotschin, S., Eakin, G. S. and Hadjantonakis, A.-K.** (2009). Dual transgene strategy for live
888 visualization of chromatin and plasma membrane dynamics in murine embryonic stem cells
889 and embryonic tissues. *genesis* **47**, 330–336.

890 **Ombrato, L., Nolan, E., Kurelac, I., Mavousian, A., Bridgeman, V. L., Heinze, I., Chakravarty, P.,**
891 **Horswell, S., Gonzalez-Gualda, E., Matacchione, G., et al.** (2019). Metastatic-niche labelling
892 reveals parenchymal cells with stem features. *Nature* **572**, 603–608.

893 **Pera, M. F. and Tam, P. P. L.** (2010). Extrinsic regulation of pluripotent stem cells. *Nature* **465**, 713–
894 720.

895 **Perez, S. E., Rebelo, S. and Anderson, D. J.** (1999). Early specification of sensory neuron fate
896 revealed by expression and function of neurogenins in the chick embryo. *Development* **126**,
897 1715–1728.

898 **Pfaff, N., Lachmann, N., Ackermann, M., Kohlscheen, S., Brendel, C., Maetzig, T., Niemann, H.,**
899 **Antoniou, M. N., Grez, M., Schambach, A., et al.** (2013). A ubiquitous chromatin opening
900 element prevents transgene silencing in pluripotent stem cells and their differentiated
901 progeny. *STEM CELLS* **31**, 488–499.

902 **Pfeifer, A., Ikawa, M., Dayn, Y. and Verma, I. M.** (2002). Transgenesis by lentiviral vectors: lack of
903 gene silencing in mammalian embryonic stem cells and preimplantation embryos.
904 *Proceedings of the National Academy of Sciences of the United States of America* **99**, 2140–
905 2145.

906 **Posfai, E., Lanner, F., Mulas, C. and Leitch, H. G.** (2021). All models are wrong, but some are useful:
907 Establishing standards for stem cell-based embryo models. *Stem Cell Reports* **16**, 1117–1141.

908 **Rao, C., Malaguti, M., Mason, J. O. and Lowell, S.** (2020). The transcription factor E2A drives neural
909 differentiation in pluripotent cells. *Development*.

910 **Rhee, J. M., Pirity, M. K., Lackan, C. S., Long, J. Z., Kondoh, G., Takeda, J. and Hadjantonakis, A.-K.**
911 (2006). In vivo imaging and differential localization of lipid-modified GFP-variant fusions in
912 embryonic stem cells and mice. *genesis* **44**, 202–218.

913 **Rossant, J. and Tam, P. P. L.** (2009). Blastocyst lineage formation, early embryonic asymmetries and
914 axis patterning in the mouse. *Development* **136**, 701–713.

915 **Roybal, K. T., Williams, J. Z., Morsut, L., Rupp, L. J., Kolinko, I., Choe, J. H., Walker, W. J., McNally,**
916 **K. A. and Lim, W. A.** (2016). Engineering T Cells with Customized Therapeutic Response
917 Programs Using Synthetic Notch Receptors. *Cell* **167**, 419–432.e16.

918 **Sancho, M., Di-Gregorio, A., George, N., Pozzi, S., Sánchez, J. M., Pernaute, B. and Rodríguez, T. A.**
919 (2013). Competitive Interactions Eliminate Unfit Embryonic Stem Cells at the Onset of
920 Differentiation. *Developmental Cell* **26**, 19–30.

921 **Santorelli, M., Lam, C. and Morsut, L.** (2019). Synthetic development: building mammalian
922 multicellular structures with artificial genetic programs. *Curr Opin Biotechnol* **59**, 130–140.

923 **Schlissel, G. and Li, P.** (2020). Synthetic Developmental Biology: Understanding Through
924 Reconstitution. *Annu. Rev. Cell Dev. Biol.* **36**, 339–357.

925 **Schultz, R. M.** (1985). Roles of Cell-to-Cell Communication in Development. *Biology of Reproduction*
926 **32**, 27–42.

927 **Seibler, J., Küter-Luks, B., Kern, H., Streu, S., Plum, L., Mauer, J., Kühn, R., Brüning, J. C. and**
928 **Schwenk, F.** (2005). Single copy shRNA configuration for ubiquitous gene knockdown in
929 mice. *Nucleic Acids Research* **33**, e67–e67.

930 **Sekine, R., Shibata, T. and Ebisuya, M.** (2018). Synthetic mammalian pattern formation driven by
931 differential diffusivity of Nodal and Lefty. *Nat Commun* **9**, 5456.

932 **Sevcsik, E., Brameshuber, M., Fölser, M., Weghuber, J., Honigmann, A. and Schütz, G. J.** (2015).
933 GPI-anchored proteins do not reside in ordered domains in the live cell plasma membrane.
934 *Nature Communications* **6**, 6969.

935 **Sgodda, M., Alfken, S., Schambach, A., Eggenschwiler, R., Fidzinski, P., Hummel, M. and Cantz, T.**
936 (2020). Synthetic Notch-Receptor-Mediated Transmission of a Transient Signal into
937 Permanent Information via CRISPR/Cas9-Based Genome Editing. *Cells* **9**, 1929.

938 **Shcherbo, D., Murphy, C. S., Ermakova, G. V., Solovieva, E. A., Chepurnykh, T. V., Shcheglov, A. S.,**
939 **Verkhusha, V. V., Pletnev, V. Z., Hazelwood, K. L., Roche, P. M., et al.** (2009). Far-red
940 fluorescent tags for protein imaging in living tissues. *Biochemical Journal* **418**, 567–574.

941 **Shioi, G., Kiyonari, H., Abe, T., Nakao, K., Fujimori, T., Jang, C.-W., Huang, C.-C., Akiyama, H.,**
942 **Behringer, R. R. and Aizawa, S.** (2011). A mouse reporter line to conditionally mark nuclei
943 and cell membranes for in vivo live-imaging. *Genesis* **49**, 570–578.

944 **Smithies, O., Gregg, R. G., Boggs, S. S., Koralewski, M. A. and Kucherlapati, R. S.** (1985). Insertion of
945 DNA sequences into the human chromosomal ß-globin locus by homologous recombination.
946 *Nature* **317**, 230–234.

947 **Srivastava, S., Salter, A. I., Liggitt, D., Yechan-Gunja, S., Sarvothama, M., Cooper, K., Smythe, K. S.,**
948 **Dudakov, J. A., Pierce, R. H., Rader, C., et al.** (2019). Logic-Gated ROR1 Chimeric Antigen
949 Receptor Expression Rescues T Cell-Mediated Toxicity to Normal Tissues and Enables
950 Selective Tumor Targeting. *Cancer Cell* **35**, 489–503.e8.

951 **Stern, C.** (1936). Somatic Crossing Over and Segregation in Drosophila Melanogaster. *Genetics* **21**,
952 625–730.

953 **Tam, P. P. L. and Loebel, D. A. F.** (2007). Gene function in mouse embryogenesis: get set for
954 gastrulation. *Nature Reviews Genetics* **8**, 368–381.

955 **Tang, R., Murray, C. W., Linde, I. L., Kramer, N. J., Lyu, Z., Tsai, M. K., Chen, L. C., Cai, H., Gitler, A.**
956 **D., Engleman, E., et al.** (2020). A versatile system to record cell-cell interactions. *eLife* **9**,
957 e61080.

958 **Tchorz, J. S., Suply, T., Ksiazek, I., Giachino, C., Cloëtta, D., Danzer, C.-P., Doll, T., Isken, A.,**
959 **Lemaistre, M., Taylor, V., et al.** (2012). A Modified RMCE-Compatible Rosa26 Locus for the
960 Expression of Transgenes from Exogenous Promoters. *PLOS ONE* **7**, e30011.

961 **Toda, S., Blauch, L. R., Tang, S. K. Y., Morsut, L. and Lim, W. A.** (2018). Programming self-organizing
962 multicellular structures with synthetic cell-cell signaling. *Science* **361**, 156–162.

963 **Toda, S., McKeithan, W. L., Hakkinen, T. J., Lopez, P., Klein, O. D. and Lim, W. A.** (2020). Engineering
964 synthetic morphogen systems that can program multicellular patterning. *Science* **370**, 327–
965 331.

966 **Tosti, L., Ashmore, J., Tan, B. S. N., Carbone, B., Mistri, T. K., Wilson, V., Tomlinson, S. R. and Kaji,**
967 **K.** (2018). Mapping transcription factor occupancy using minimal numbers of cells in vitro
968 and in vivo. *Genome Research* **28**, 592–605.

969 **Toth, T., Balassa, T., Bara, N., Kovacs, F., Kriston, A., Molnar, C., Haracska, L., Sukosd, F. and**
970 **Horvath, P.** (2018). Environmental properties of cells improve machine learning-based
971 phenotype recognition accuracy. *Scientific Reports* **8**, 10085.

972 **Velkey, J. M. and O'Shea, K. S.** (2013). Expression of Neurogenin 1 in Mouse Embryonic Stem Cells
973 Directs the Differentiation of Neuronal Precursors and Identifies Unique Patterns of Down-
974 stream Gene Expression. *Developmental Dynamics* **242**, 230–253.

975 **Wang, L., Long, J., Chen, H., Sun, S., Lv, K., Li, Q. and Wang, X.** (2021). Manipulation of focal Wnt
976 activity via synthetic cells in a double-humanized zebrafish model of tumorigenesis.
977 *International Journal of Cancer* **148**, 2815–2824.

978 **Whittingham, D. G.** (1974). Embryo banks in the future of developmental genetics. *Genetics* **78**,
979 395–402.

980 **Wu, G., Liu, N., Rittelmeyer, I., Sharma, A. D., Sgodda, M., Zaehres, H., Bleidißel, M., Greber, B.,**
981 **Gentile, L., Han, D. W., et al.** (2011). Generation of Healthy Mice from Gene-Corrected
982 Disease-Specific Induced Pluripotent Stem Cells. *PLOS Biology* **9**, e1001099.

983 **Yang, Z., Yu, Z., Cai, Y., Du, R. and Cai, L.** (2020). Engineering of an enhanced synthetic Notch
984 receptor by reducing ligand-independent activation. *Communications Biology* **3**, 1–7.

985 **Yang, B. A., Westerhof, T. M., Sabin, K., Merajver, S. D. and Aguilar, C. A.** (2021). Engineered Tools
986 to Study Intercellular Communication. *Advanced Science* **8**, 2002825.

987 **Yuan, L. and Hassan, B. A.** (2014). Neurogenins in brain development and disease: An overview.
988 *Archives of Biochemistry and Biophysics* **558**, 10–13.

989 **Zhu, I., Liu, R., Hyrenius-Wittsten, A., Piraner, D. I., Alavi, J., Israni, D. V., Khalil, A. S. and Roybal, K.**
990 **T.** (2021). Design and modular assembly of synthetic intramembrane proteolysis receptors
991 for custom gene regulation in therapeutic cells. *bioRxiv* 2021.05.21.445218.

992

993 **FIGURE LEGENDS**

994 **Figure 1. Diagram of SynNotch cell-cell interaction reporter ES cells.**
995 (A) Interaction between a membrane-tethered ligand and the Notch receptor extracellular domain
996 leads to the cleavage of the Notch core transmembrane domain, which contains proteolytic cleavage
997 sites. In turn, this leads to the release of the Notch intracellular domain from the membrane,
998 allowing it to translocate to the nucleus and drive transcription of target genes. (B) Sender cells
999 express membrane-tethered extracellular EGFP from a ubiquitous promoter. (C) Receiver cells
1000 contain a *TRE-mCherry* transgene, express *tagBFP-3xNLS* from a ubiquitous promoter, and express a
1001 SynNotch receptor from a ubiquitous promoter. The SynNotch receptor is comprised of an
1002 extracellular LaG17 anti-GFP nanobody, the core transmembrane region of Notch1, and an
1003 intracellular tTA. (D) Upon interaction of the EGFP on a sender cell with the SynNotch receptor, the
1004 Notch1 core domain is cleaved, releasing the tTA, which can translocate into the nucleus, bind the
1005 TRE element, and drive *mCherry* transcription.

1006 **Figure 2. Screening of clonal sender ESC lines.**
1007 (A-D) Diagram of the constructs used to generate EGFP sender cell lines. (E) Median EGFP intensity
1008 and (G) percentage EGFP-positive cells in untagged EGFP sender cells. Parental wild-type cells are
1009 included as a negative control. 5000 cells were analysed for each clone. (F) Median EGFP intensity
1010 and (H) percentage EGFP-positive cells in HA- and Myc-tagged EGFP sender cells. Parental wild-type
1011 cells are included as a negative control. 15000 cells were analysed for each clone. Analyses were
1012 performed separately from those in (E), median intensities are not directly comparable. For panels
1013 (E-H), n=1. (I) Comparison of EGFP distributions in parental wild-type cells, CmGP clone 1 (CmGP1)
1014 and CHmGMP clone 19 (CHmGMP19) sender cells. 85000 cells were analysed for each sample. Data
1015 from a single experiment, representative of 9 biological replicates. (J) Immunofluorescence of
1016 parental wild-type, CmGP1 and CHmGMP19 sender cells. Scale bar: 30µm. Nuclei: LaminB1. A.F.U.:
1017 arbitrary fluorescence units.

1018 **Figure 3. Generation of clonal cell-cell interaction reporter STC receiver cells.**
1019 (A) Summary of transgenes stably integrated into the genome of STC clonal ESC lines. (B-C) Flow
1020 cytometry analysis of mCherry and tagBFP-3xNLS expression in (B) wild-type and (C) control PSNBB-E
1021 cells containing all SyNPL receiver constructs except for the TRE-mCherry cassette. These control cell
1022 lines were used to set gates for tagBFP- and mCherry-positivity. (D) Immunofluorescence of STC
1023 clones A1, B1 and B2 co-cultured with CmGP1 sender cells for 24 hours (1:3 sender:receiver cell
1024 ratio). Scale bar: 30µm. (E-H) Flow cytometry analysis of mCherry and tagBFP-3xNLS expression in
1025 STC receiver cells cultured alone or in the presence of indicated EGFP-expressing cell lines (9:1
1026 sender:receiver cell ratio). The mCherry-HI gate displayed in figure was set based on mCherry
1027 distribution in STC receiver cells cultured alone. Data in these panels were acquired simultaneously
1028 to data in panels (B,C) and can be directly compared.
1029 For panels (B,C,E-H) percentages of cells in each gate are indicated. 11000 cells were analysed for
1030 each sample. Data from a single experiment, representative of 4 biological replicates. Diagrams
1031 depicting the transgenes present in each cell type and expected mCherry and tagBFP-3xNLS
1032 expression patterns are displayed next to flow cytometry plots.

1033 **Figure 4. Kinetics of mCherry induction in STC receiver cells.**
1034 (A) Stills from Movie 1 displaying mCherry and EGFP expression in STC clone A1 receiver cells co-
1035 cultured with CmGP1GH1 sender cells (1:1 sender:receiver cell ratio). Immuofluorescence of cells
1036 after 24 hours of filming is displayed as a 24 hour timepoint, and includes tagBFP-3xNLS signal in
1037 place of a brightfield image. Scale bar: 30µm. Yellow arrowheads: initial STC receiver cell contact
1038 with sender cells, onset of mCherry expression, cell descendants at 24 hours. Magenta arrowheads:

1039 STC receiver cell not making contact with sender cells, cell descendants at 24 hours. Cyan
1040 arrowhead: initial STC receiver cell contact with sender cell, cell descendant at 24 hours.
1041 (B) Stills from Movie 2 displaying tagBFP-3xNLS, mCherry and EGFP expression in STC clone A1
1042 receiver cells co-cultured with CmGP1GH1 sender cells (9:1 sender:receiver cell ratio). Scale bar:
1043 30µm.
1044 (C) Experimental setup to analyse kinetics of mCherry upregulation in STC receiver cells by flow
1045 cytometry.
1046 (D) Percentage of mCherry-HI STC receiver cells following co-culture with CmGP1 sender cells for the
1047 indicated amount of time (9:1 sender:receiver cell ratio). Data presented as mean ± standard
1048 deviation of three independent experiments. A minimum of 8000 cells were analysed for each
1049 sample. The mCherry-HI gate was set based on mCherry distribution in STC receiver cells cultured
1050 alone.
1051 (E) Distribution of mCherry fluorescence in STC clone A1 receiver cells following co-culture with
1052 CmGP1 sender cells for the indicated amount of time (9:1 sender:receiver cell ratio). Data from a
1053 single experiment, representative of three biological replicates. STC clone A1 cells cultured alone
1054 ("0h") are displayed as a shaded black histogram in all panels. 10000 cells were analysed for each
1055 sample.
1056 (F) Quantification of live imaging: median mCherry fluorescence intensity in STC clone A1 receiver
1057 cells following co-culture with CmGP1GH1 or E14GIP1 cells for the indicated amount of time (9:1
1058 sender:receiver cell ratio). Average of 3 biological replicates, 10 random fields of view/replicate,
1059 minimum of 320 cells/replicate/timepoint. Error bars: standard deviation.
1060 (G) Mean mCherry fluorescence intensity in individual STC clone A1 receiver cells tracked for 24
1061 hours whilst in co-culture with CmGP1GH1 sender cells (9:1 sender:receiver ratio). Tracks are
1062 displayed for 33 randomly selected cells for each of 3 biological replicates (99 cells total). Mean, 10th,
1063 and 90th centile tracks are also displayed.
1064 A.F.U.: arbitrary fluorescence units.
1065
1066 **Figure 5. Characterisation of minimal contact time required for mCherry induction in STC receiver**
1067 **cells.**
1068 (A) Stills from Movie 3 displaying mCherry and EGFP expression in STC clone A1 receiver cells co-
1069 cultured with CmGP1GH1 sender cells (1:1 sender:receiver cell ratio). Immuofluorescence of cells
1070 after 24 hours of filming is displayed as a 24 hour timepoint, and includes tagBFP-3xNLS signal in
1071 place of a brightfield image. Scale bar: 30µm. White arrowheads label an STC receiver cell in contact
1072 with sender cells for 7 hours, which then loses contact with sender cells between the 8 and 20 hour
1073 timepoints whilst its levels of mCherry keep increasing. (B) Experimental setup to analyse kinetics of
1074 mCherry upregulation in STC receiver cells by flow cytometry, allowing time for protein maturation.
1075 Following sender:receiver cell co-culture for 0-24 hours, 1µg/ml doxycycline (dox) was added to the
1076 culture medium for a further 16 hours in order to inhibit tTA-mediated *mCherry* transcription, and
1077 allow translation and folding of previously transcribed *mCherry*.
1078 (C) Percentage of mCherry-HI STC receiver cells after co-culture with CmGP1 sender cells for the
1079 indicated amount of time and following a further 16 hours of doxycycline treatment (9:1
1080 sender:receiver cell ratio). Data presented as mean ± standard deviation of three independent
1081 experiments. A minimum of 8000 cells were analysed for each sample. The mCherry-HI gate was set
1082 based on mCherry distribution in STC receiver cells cultured alone in doxycycline for 16 hours.
1083 (D) Distribution of mCherry fluorescence in STC clone A1 receiver cells following co-culture with
1084 CmGP1 sender cells for the indicated amount of time and 16 hours doxycycline treatment (9:1
1085 sender:receiver cell ratio). Data from a single experiment, representative of three biological
1086 replicates. STC clone A1 cells plated with CmGP1 sender cells in doxycycline-containing medium for
1087 16 hours ("0h") are displayed as a shaded black histogram in all panels. 10000 cells were analysed
1088 for each sample.
1089

1090 **Figure 6. Contact-mediated induction of mCherry in chimaeric blastocysts.**
1091 (A) Chimaeric blastocysts containing STC clone B1 receiver cells and/or CmGP1GH1 sender cells. The
1092 images of the three embryos were taken from the same z-plane of a confocal stack and come from a
1093 single field of view. Nuclei were counterstained with DRAQ7. Scale bars: 30µm. (B) Quantification of
1094 embryos containing cells expressing readily detectable levels of mCherry ("mCherry-HI") across all
1095 experiments. Embryos containing both sender and receiver cells were used as a reference for scoring
1096 sender-only chimaeras, receiver-only chimaeras, and wild-type embryos.

1097 **Figure 7. Contact-mediated synthetic patterning of gene expression and fate programming.**
1098 (A) Diagram illustrating synthetic patterning strategy: sender and receiver cells are grown to
1099 confluence in separate chambers of a multi-chamber culture insert. The insert is removed and cells
1100 are allowed to proliferate until they come into contact, which induces transgene expression in
1101 receiver cells in a stripe pattern. (B) Synthetic striped pattern of mCherry induction in STC clone B1
1102 receiver ESCs in contact with CmGP1 sender ESCs. EGFP, tagBFP, mCherry immunofluorescence. (C)
1103 Summary of transgenes stably integrated into the genome of *Neurog1*-inducible STN clonal ESC lines.
1104 (D) Synthetic striped pattern of neuronal differentiation of STN receiver ES cells in contact with
1105 CmGP1 sender ESCs. EGFP, tagBFP, Tubb3 immunofluorescence. Scale bars: 30µm.

FIGURE 1

A Notch signalling

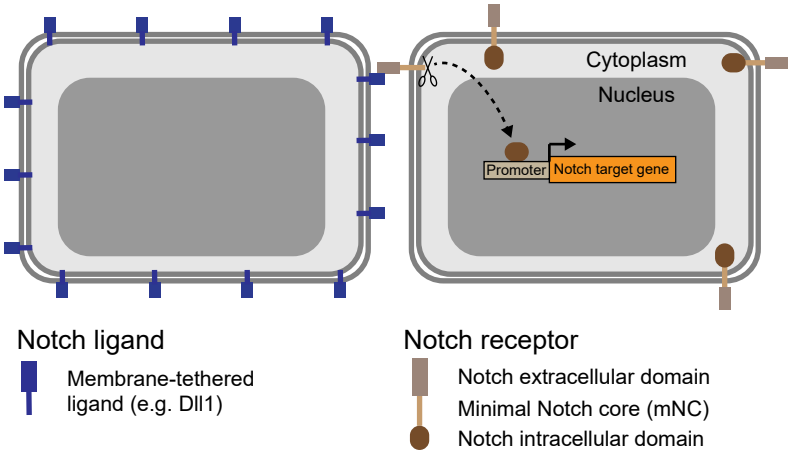

B SyNPL sender cells

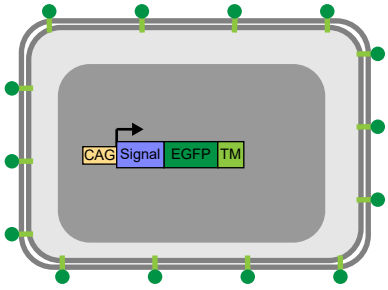

C SyNPL receiver cells

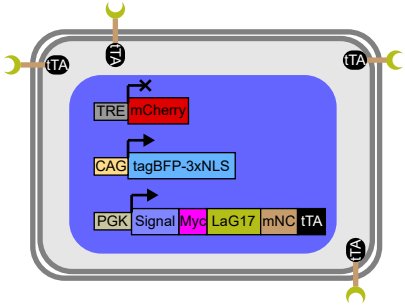

D Sender cells in direct contact with receiver cells

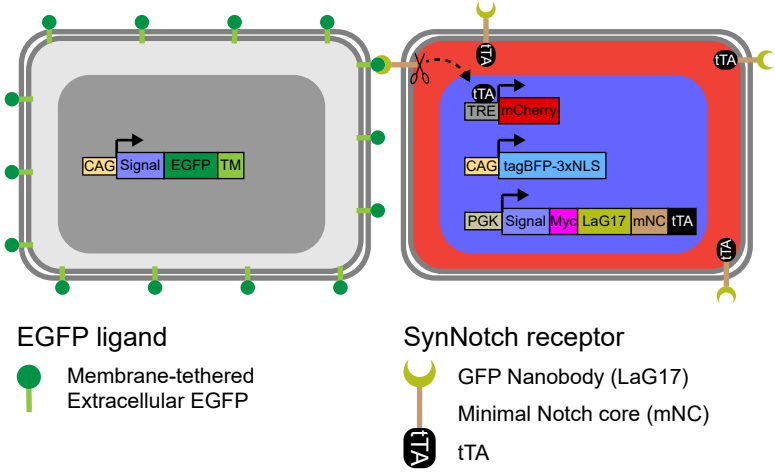

FIGURE 2

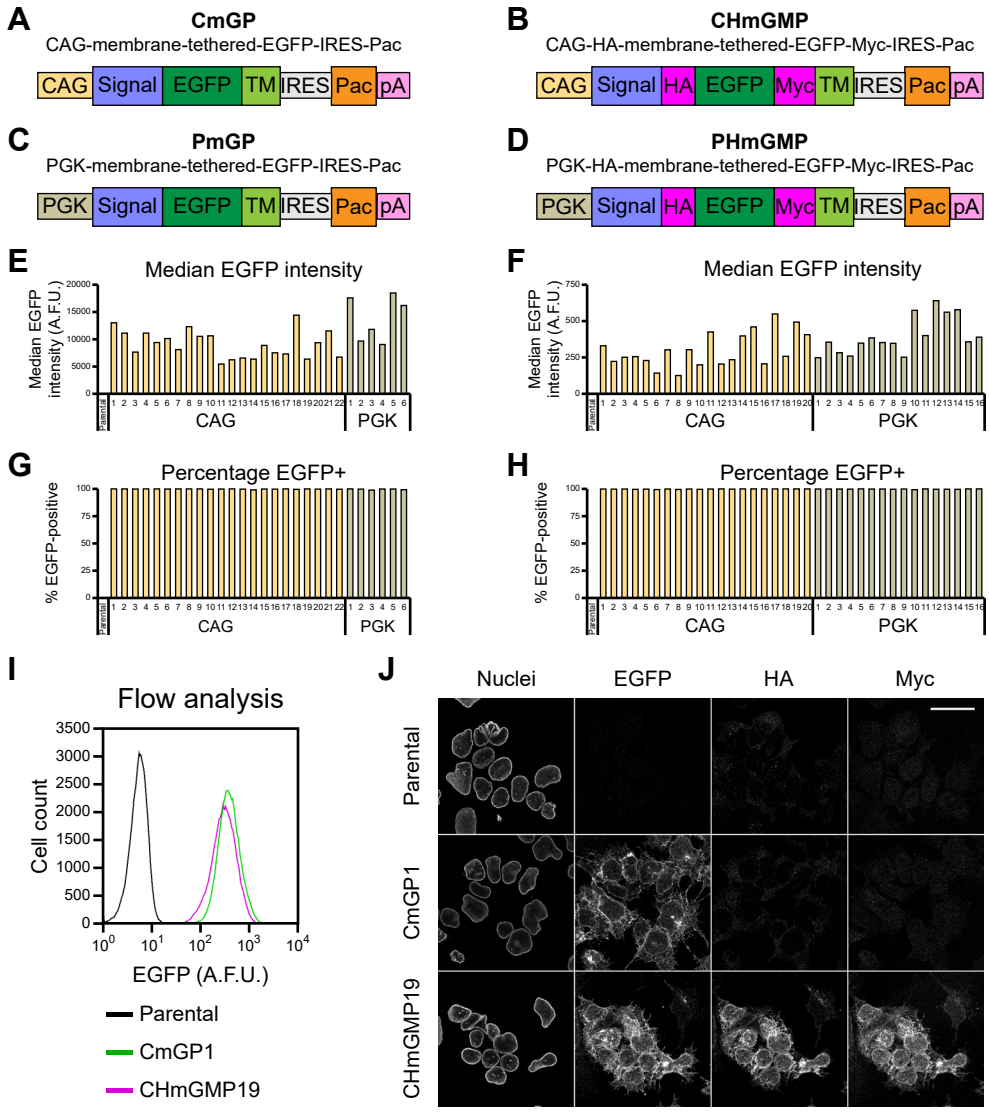
A
CmGP
CAG-membrane-tethered-EGFP-IRES-Pac
CAG Signal EGFP TM IRES Pac pA
B
CHmGMP
CAG-HA-membrane-tethered-EGFP-Myc-IRES-Pac
CAG Signal HA EGFP Myc TM IRES Pac pA
C
PmGP
PGK-membrane-tethered-EGFP-IRES-Pac
PGK Signal EGFP TM IRES Pac pA
D
PHmGMP
PGK-HA-membrane-tethered-EGFP-Myc-IRES-Pac
PGK Signal HA EGFP Myc TM IRES Pac pA
E
Median EGFP intensity
Median EGFP intensity (A.F.U.)
Parental
CAG
PGK
F
Median EGFP intensity
Median EGFP intensity (A.F.U.)
Parental
CAG
PGK
G
Percentage EGFP+
% EGFP-positive
Parental
CAG
PGK
H
Percentage EGFP+
% EGFP-positive
Parental
CAG
PGK
I
Flow analysis
Cell count
EGFP (A.F.U.)
Parental
CmGP1
CHmGMP19
J
Nuclei
EGFP
HA
Myc
Parental
CmGP1
CHmGMP19

FIGURE 3

A

STC receiver cells (SynNotch-TRE-mCherry)

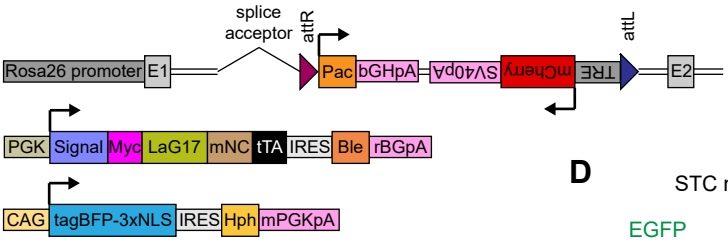

B

Wild-type

C

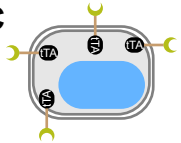

EV control "receivers"

Flow analysis of EGFP- cells

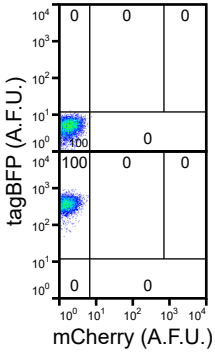

D

STC receivers + CmGP1 senders

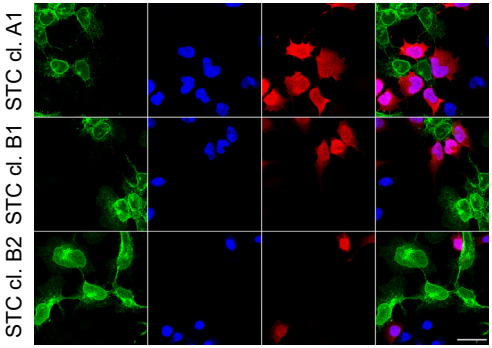

E

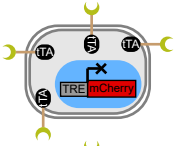

STC receivers

F

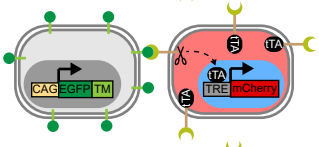

STC receivers + CmGP1 senders

G

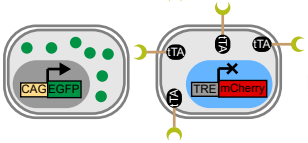

STC receivers + E14GIP1 "senders"

H

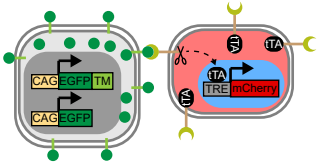

STC receivers + CmGP1GH1 senders

Flow analysis of tagBFP+ EGFP- cells

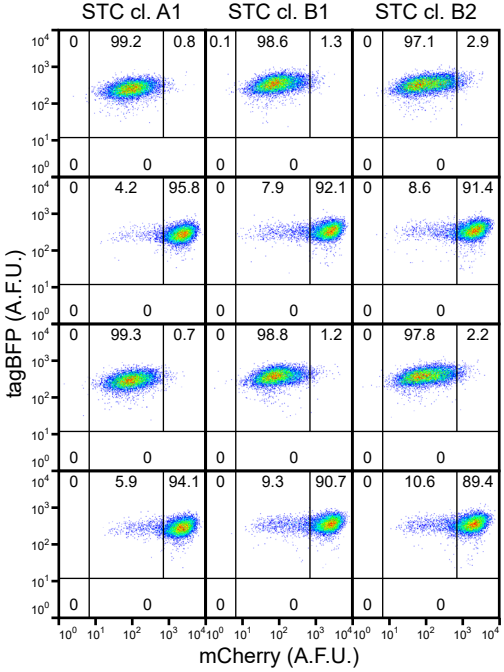

FIGURE 4

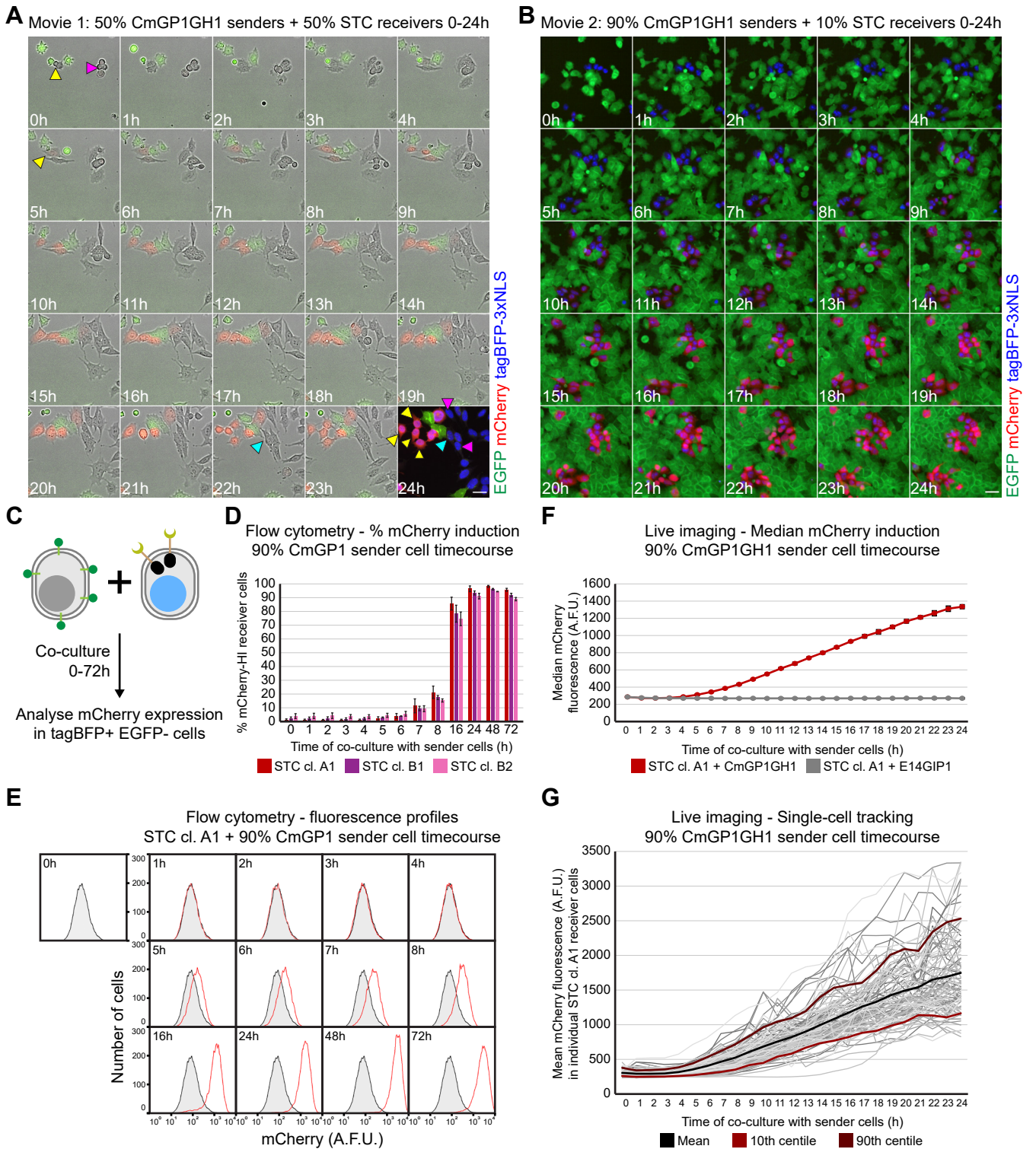
A
Movie 1: 50% CmGP1GH1 senders + 50% STC receivers 0-24h
0h
1h
2h
3h
4h
5h
6h
7h
8h
9h
10h
11h
12h
13h
14h
15h
16h
17h
18h
19h
20h
21h
22h
23h
24h
EGFP mCherry tagBFP-3xNLS
B
Movie 2: 90% CmGP1GH1 senders + 10% STC receivers 0-24h
EGFP mCherry tagBFP-3xNLS
C
Co-culture
0-72h
Analyse mCherry expression
in tagBFP+ EGFP- cells
D
Flow cytometry - % mCherry induction
90% CmGP1 sender cell timecourse
% mCherry-HI receiver cells
Time of co-culture with sender cells (h)
STC cl. A1
STC cl. B1
STC cl. B2
F
Live imaging - Median mCherry induction
90% CmGP1GH1 sender cell timecourse
Median mCherry
fluorescence (A.F.U.)
Time of co-culture with sender cells (h)
STC cl. A1 + CmGP1GH1
STC cl. A1 + E14GIP1
E
Flow cytometry - fluorescence profiles
STC cl. A1 + 90% CmGP1 sender cell timecourse
Number of cells
mCherry (A.F.U.)
G
Live imaging - Single-cell tracking
90% CmGP1GH1 sender cell timecourse
Mean mCherry fluorescence (A.F.U.)
in individual STC cl. A1 receiver cells
Time of co-culture with sender cells (h)
Mean
10th centile
90th centile

FIGURE 5

A Movie 3: 50% CmGP1GH1 senders + 50% STC receivers 0-24h

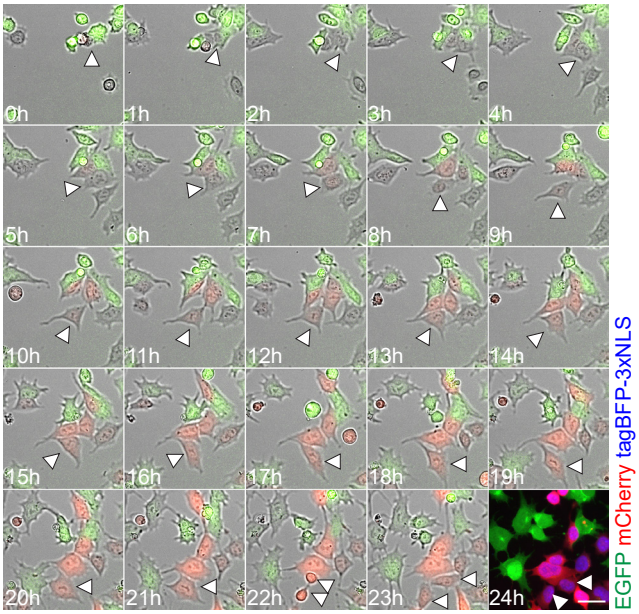

B

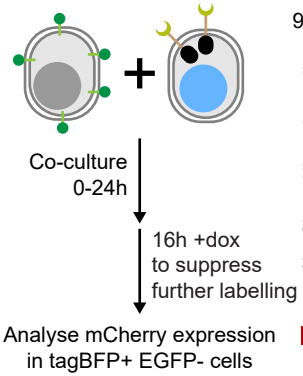

C

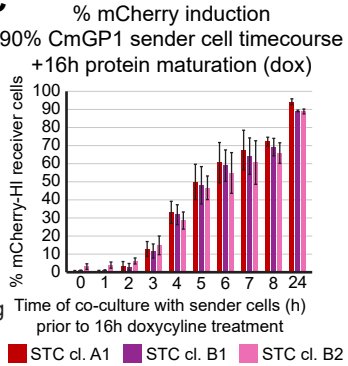

D

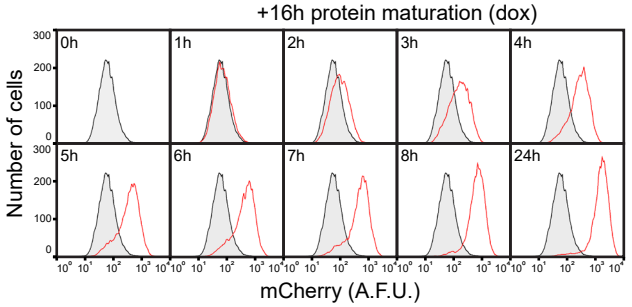

Timepoints refer to initial duration of dox-free co-culture permissive for mCherry induction prior to addition of dox for 16h

FIGURE 6

A

Chimaeric blastocysts with STC receiver + CmGP1GH1 sender cells

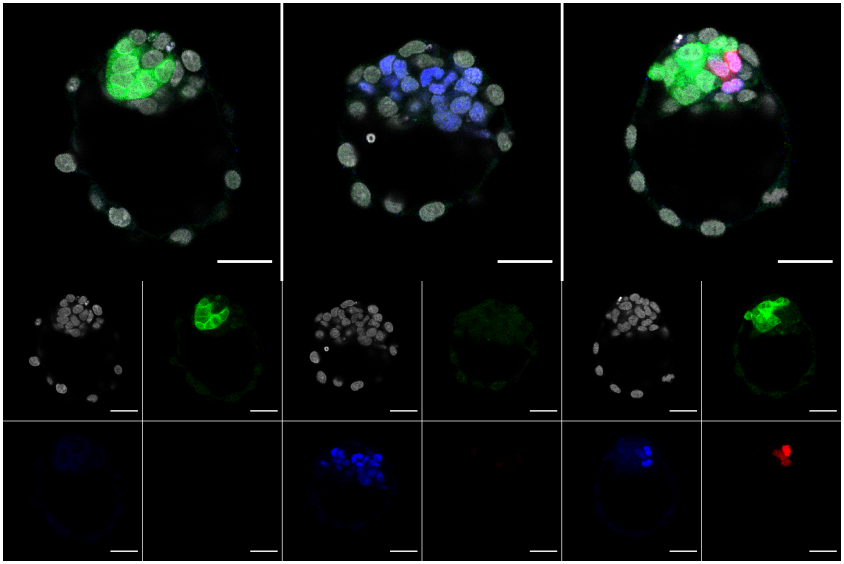

Nuclei EGFP tagBFP-3xNLS mCherry

B

	mCherry-HI embryos / total embryos			
	All clones	STC cl. A1	STC cl. B1	STC cl. B2
Wild-type	**0/11**	-	-	-
Senders only	**0/27**	-	-	-
Receivers only	**1/19**	1/13	0/3	0/3
Receivers+senders	**80/80**	56/56	23/23	11/11

FIGURE 7

A

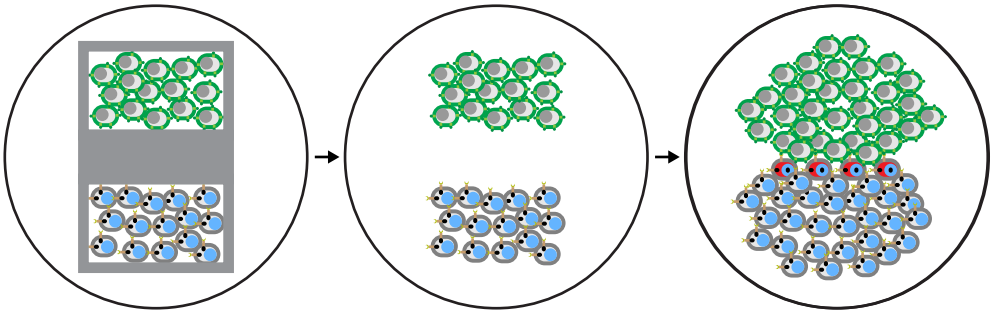

Plate sender and receiver cells in separate wells of multiwell insert

Remove multiwell insert
Give cells time to proliferate

Transgene expression induced at linear interface between sender and receiver cells

B

mCherry induction in STC receivers at sender-receiver border

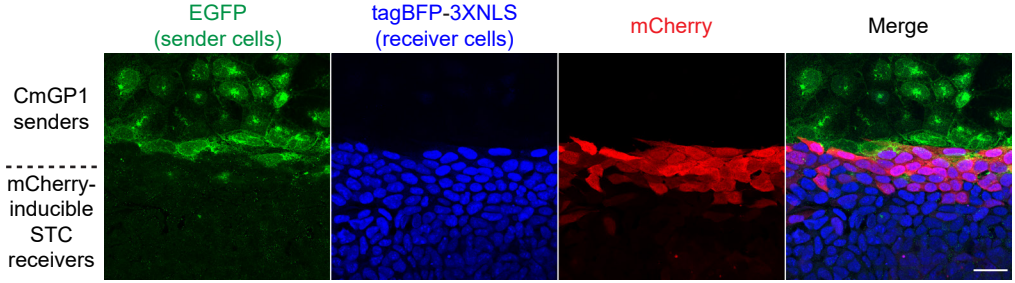

C

STN receiver cells (Neurog1-inducible)

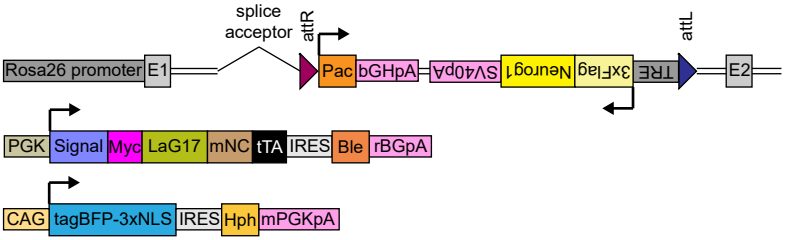

D
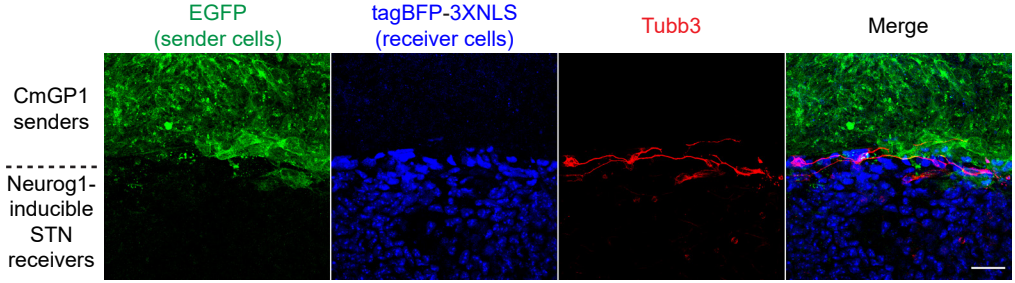
Forced neuronal differentiation of STN receivers at sender-receiver border